Postimpact modification by volcanic or tectonic processes as the rule, not the exception, for Venusian craters

Robert R. Herrick[1] and M. Elise Rumpf[2,3]

Received 26 August 2010; revised 4 November 2010; accepted 16 November 2010; published 10 February 2011.

[1] We present three investigations that use the Venusian impact crater population to constrain the planet's resurfacing history. We evaluate stereo-derived topography for 91 Venusian craters that have a diameter (D) greater than 15 km. Craters with radar-bright floors have greater rim-floor depths and rim heights than craters with radar-dark floors. For the bright-floored craters rim-floor depths are $d_{bf} = 0.483\ D^{0.165}$ and rim heights are $rh_{bf} = 0.056\ D^{0.483}$. Trends for dark-floored craters are $d_{df} = 0.424\ D^{0.108}$ and $rh_{df} = 0.181\ D^{-0.025}$. For a 60 km crater, this represents differences of 290 m in rim-floor depth and 240 m in rim height. We interpret these results to indicate that dark-floored craters have experienced postimpact volcanic embayment and filling. We examine the population of craters with D > 20 km that have radar-dark halos surrounding their continuous ejecta (114 craters). We find that a portion of the halo has been removed for almost all dark-floored craters, consistent with our interpretation that dark-floored craters have been affected by postimpact volcanism. Finally, we assessed geologic histories of 12 large impact structures with stereo coverage. All but one of these structures has experienced postimpact volcanism or tectonic deformation, often in multiple episodes. In summary, widespread volcanic and tectonic activity occurred throughout the time period of emplacement of the crater population. Postulated resurfacing histories that consider the majority of craters to be at the top of the stratigraphic column are invalid, and the mean surface age of Venus is young (~150 My).

Citation: Herrick, R. R., and M. E. Rumpf (2011), Postimpact modification by volcanic or tectonic processes as the rule, not the exception, for Venusian craters, *J. Geophys. Res.*, *116*, E02004, doi:10.1029/2010JE003722.

1. Introduction

[2] The global distribution of impact craters on Venus is one of the more surprising results from the Magellan mission to Venus. The distribution, taken by itself, is statistically consistent with a random population emplaced on a Venusian surface with a mean age of a few hundred million years [*Phillips et al.*, 1992; *Schaber et al.*, 1992; *McKinnon et al.*, 1997]. Two conceptual end-member resurfacing models were developed to describe the distribution [*Phillips et al.*, 1992]. Here we define the term "resurfacing" to mean to cover a surface or so heavily deform it that its previous appearance is unrecognizable. Geologic activity that renders a crater unidentifiable can be generically termed a "resurfacing event." In one end-member, a spatially random distribution of craters can be maintained by having short duration resurfacing events of large spatial area occur in random locations with long intervening time intervals. A special case of this end-member would be global resurfacing events; for this special case we would be unable to tell from the current surface whether the last global event was part of a recurring cycle or a singular event in the planet's history. The other end-member is that resurfacing events that wipe out craters are of small spatial area, randomly distributed, and frequently occurring. That end-member is effectively an uniformitarian hypothesis as it assumes that geologic activity is occurring everywhere at similar rates.

[3] Because the resurfacing events have a finite duration, the end-member models can be distinguished by the percentage of craters that are in the process of getting eliminated. Global events that periodically resurface nearly the entire planet will leave a crater-free surface; craters then occur and are subsequently unmodified until the next global event. Resurfacing events occurring frequently everywhere will produce a surface with many craters in the process of being resurfaced. In geologic terms, we can thus distinguish the end-members by observing the extent to which the craters have experienced some degree of tectonic deformation or volcanic flooding. Initial surveys of the crater population suggested that only a few percent of the craters were heavily deformed or embayed by subsequent volcanism [*Schaber et al.*, 1992; *Phillips et al.*, 1992; *Herrick and Phillips*, 1994; *Strom et al.*, 1994; *Collins et al.*, 1999], thus favor-

[1]Geophysical Institute, University of Alaska Fairbanks, Fairbanks, Alaska, USA.
[2]State University of New York at Buffalo, Buffalo, New York, USA.
[3]Now at Hawai'i Institute of Geophysics and Planetology, University of Hawai'i at Manoa, Honolulu, Hawaii, USA.

0148-0227/11/2010JE003722

ing the "catastrophic resurfacing" end-member. A number of geophysical models were proposed to generate a global catastrophe, including episodic plate tectonics [*Turcotte*, 1993], a transition from mobile lid to stagnant lid convection [e.g., *Solomatov and Moresi*, 1996], and a rapid transition from a thin to thick lithosphere [e.g., *Reese et al.*, 2007].

[4] Some statistically significant nonrandomness to the distribution was observed when the distribution of craters was considered in the context of the geologic features on Venus. The portion of the planet with large rift zones and superposed large volcanoes was found to correlate with a low crater density and an unusual number of heavily deformed and obviously embayed craters [*Namiki and Solomon*, 1994; *Herrick and Phillips*, 1994]. The tessera regions of the planet seem to have a slightly higher than normal percentage of craters, but few of these craters appear to be heavily deformed [*Ivanov and Basilevsky*, 1993]. These observations (and many others not elaborated upon here), combined with global geologic mapping activities, led to scenarios of geologic surface evolution that paralleled the catastrophic geophysical models. The general vision is that the tessera regions are old and date to a past time of more intense surface deformation; in rapid succession the tessera ceased deforming and volcanism flooded the low-lying areas; currently limited geologic activity is concentrated along the planet's rift zones [e.g., *Basilevsky and Head*, 1995; *Herrick*, 1994; *Price and Suppe*, 1995].

[5] In a series of subsequent papers, Basilevsky and colleagues [*Basilevsky and Head*, 1998, 2000, 2002a, 2002b, 2002c, 2006; *Basilevsky et al.*, 1997, 1999] extensively developed this model that *Guest and Stofan* [1999] termed the "directional history" for Venus evolution. The general idea is that there is a global stratigraphy that progresses from heavily deformed tessera, to heavily deformed, then moderately deformed plains, and then to undeformed plains. Most recent activity is focused near major rift zones that tend to intersect with large shield volcanoes. The planet has been mapped into geomorphological units that are considered to be mostly globally synchronous. Considering the mean surface age from the cratering record as "T," they used the following techniques to estimate ages, and duration of emplacement, of their global stratigraphic units relative to T:

[6] 1. They determine the craters per unit area for a global stratigraphic unit. This provides a mean age for the unit.

[7] 2. Using such features as postcrater embayment or crosscutting by wrinkle ridges, a crater within a unit can be assessed as predating or postdating events that occurred during deposition of a unit.

[8] 3. Dark haloes and parabolas around craters are assumed to degrade in a globally consistent manner with time, so that the presence or absence of these features provides time constraints on how long the crater and its associated radar-dark feature have been on the surface.The second and third techniques constrain the duration of formation of the unit.

[9] The validity of their dating methodology requires that certain conditions must hold true. First, either most of the craters must be pristine, or the postcrater modification must be "unimportant." Otherwise, the age derived from a count of craters per unit area has no meaning. To illustrate this point, consider what would happen if one attempted to date the lunar maria by counting both postmare craters and mare-filled craters. In areas where the mare is thin (many premare craters are visible), one would have an overcount of craters and obtain an older than appropriate age for the mare. Counting only the mare-filled craters provides us no age information on the age of the premare surface, as we are not counting all those craters that were buried by the mare. In order to date the premare surface, we have to go somewhere where maria is either not present or so thin that none of the premare craters in our counting diameter range have been buried.

[10] Thus, on Venus, using crater counts to obtain a mean age for a stratigraphic unit assumes that what one is defining as a particular unit was thick enough to have completely buried all preexisting craters, and yet was emplaced rapidly enough that no craters were buried during unit formation. Even then, the unit age that is obtained neglects any volcanism that partially fills or embays craters. The second and third techniques listed above require even more rigid conditions be met. To use the total number of craters in a unit and the number of unmodified craters in a unit to bracket the beginning and end of a unit's formation requires that there is a basement unit that is thick and so rapidly emplaced that it had no craters on it, and then the unit in question formed and was thin enough not to bury any craters during formation. Using crosscutting relationships between wrinkle ridges and crater floors to date the interval between plains unit and wrinkle ridge formation further assumes that no crater floors were partially filled after wrinkle ridge formation. Using a degradation sequence for dark haloes and parabolas in order to date individual deposits assumes that haloes and parabolas are not removed by postimpact volcanism. Implicit in all of their mapping is a "tie goes to the runner" approach to assessing postimpact activity: unless unambiguous embayment or flooding is observed, a crater is assumed to be at the top of the stratigraphic column.

[11] There have been some observations of the craters that suggest that these conditions are not met, and mapping efforts of others [e.g., *Guest and Stofan*, 1999; *Stofan et al.*, 2005; *Hansen and Young*, 2007] have challenged the validity of the rapid, directional evolution viewpoint of surface geology. One problem is that most of the otherwise pristine appearing impact craters over ~15 km in diameter have floors with low backscatter relative to the rim and ejecta; the floors are similar in appearance to the volcanic plains that comprise most of the planet's surface. We refer to craters with such floors as "dark-floored" craters, in contrast to "bright-floored" craters with backscatter properties similar to the rim and ejecta (Figure 1). The rim-floor depth of an impact crater can be estimated from the offset between the geometric centers of the crater rim and floor in a single-look radar image. Utilizing this single-look technique, *Sharpton* [1994] demonstrated that dark-floored craters had shallower rim-floor depths than bright-floored craters. *Wichman* [1999] studied the morphology of Venusian crater interiors and concluded that dark-floored craters were caused by postimpact volcanic filling, and he ruled out impact melt and eolian processes as possible causes for dark floors. Using a more precise stereo radargrammetry technique than the *Sharpton* [1994] approach, *Herrick and Sharpton* [2000] showed that the bright-floored craters were not only deeper but also had higher rims than the dark-floored craters. That paper also contained an extensive discussion of hypotheses for the origin of radar-dark floors in craters, and concluded that volcanic infilling was the only viable hypothesis. Thus, the primary conclusion from *Herrick and Sharpton* [2000] was that the majority of impact craters with D > 15 km on

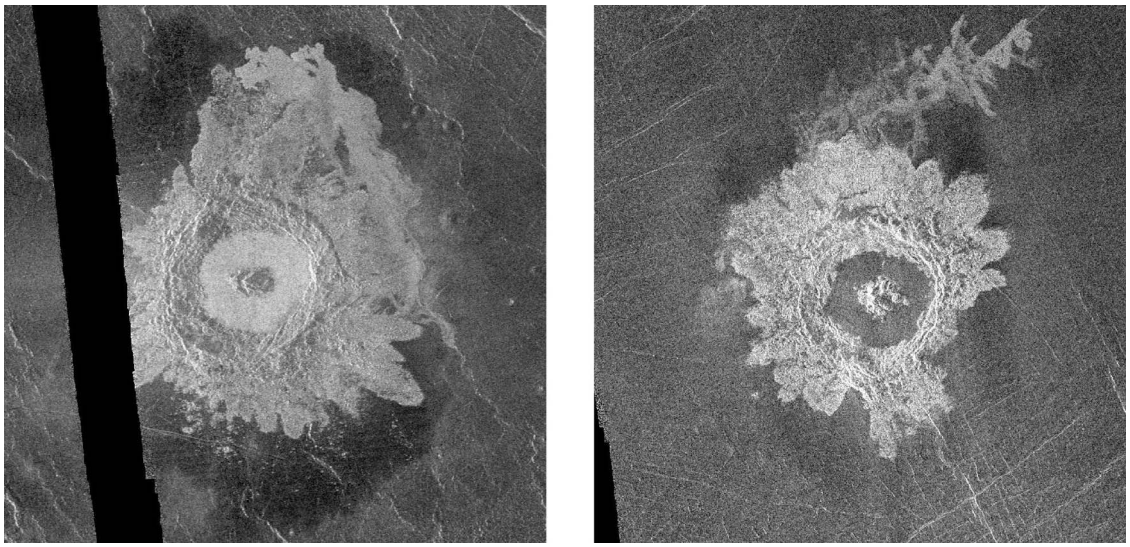

Figure 1. A (left) "bright-floored" and (right) "dark-floored" crater used in this study. The backscatter of the floor of the right crater (O'Conner, D = 30 km, located at 26.0°S, 143.9°E) is similar to the surrounding volcanic plains, but the backscatter of the left crater's floor (Bassi, D = 31 km, located at 19.0°S, 64.7°E) is high and similar to that of the ejecta blanket. The left crater is also nearly completely surrounded by a "dark halo" feature. The right crater also has what can be interpreted as a dark halo that is most prominent north and east of the bright ejecta. North is up.

Venus have experienced both infilling and exterior flooding by volcanic flows.

[12] Here we present three related investigations that explore various aspects of postimpact modification of craters. First, we update the results of *Herrick and Sharpton* [2000]. While that work showed a statistically significant difference in mean depths and rim heights between bright- and dark-floored craters, the limited number of craters studied left doubts in the minds of some critics. For D > 15 km, here we present results for all craters covered by left-left stereo imagery and bright-floored craters covered by right-left imagery. This roughly doubles the number of craters from the results of *Herrick and Sharpton* [2000].

[13] In the second investigation we address an apparent discrepancy with the hypothesis that dark-floored craters have experienced volcanic filling and embayment: the presence of dark halos around many of these craters (e.g., Figure 1). Dark halos are roughly circular, low-backscatter areas just beyond a crater's continuous ejecta. Explanations for their formation lead to the conclusion that they occur ubiquitously around Venusian craters when they form [e.g., *Phillips et al.*, 1991; *Schultz*, 1992], and craters with a dark halo are much more likely to have a bright floor [*Herrick and Phillips*, 1994]. There are, however, many dark-floored craters with dark halos [*Herrick and Phillips*, 1994], a situation that would seem to be at odds with the hypothesis that dark-floored craters have later been embayed and filled by volcanic flows. We examine the craters with D > 20 km and dark halos to evaluate whether the presence of dark halos around dark-floored craters invalidates the hypothesis that volcanic filling and embayment produces a dark floor in an impact crater.

[14] These first two investigations, involving crater depths and dark halos, involve statistical assessments of limited observations made on a large number of craters. In the third investigation, we look in detail at the geologic histories of all of the large craters (D > 45 km) for which we have substantial left-left stereo coverage. *Herrick and Sharpton* [1996] used imagery and stereo-derived topography to assess the geologic history of Mead, the largest impact basin on Venus. The high-resolution topography made evident otherwise ambiguous geologic contacts and stratigraphic relationships, and Mead was shown to have experienced partial volcanic embayment of the crater ejecta. Here we conduct similar investigations for 12 other large impact structures to assess the nature of any postimpact volcanism and deformation. While some of these structures have been part of various geologic mapping efforts, most have not been examined in detail, and none of them have previously been examined with the benefit of stereo-derived topography.

[15] Our overall approach is to combine the large sample, limited observations approach of our first two investigations with the detailed analyses involved in the third investigation to generate a comprehensive picture of postimpact crater modification on Venus. We discuss our results in the context of past and current mapping efforts and models for global resurfacing history.

2. Update on the Topography of Venusian Craters

[16] In the work of *Herrick and Sharpton* [2000], high-resolution Digital Elevation Models (DEMs) derived using stereo radargrammetric techniques were presented for 74 Venusian craters. That work contained a detailed assessment of the methodology, available data, and resolution of the resulting DEMs. Some of the relevant points regarding stereo-derived DEMs for impact craters are as follows:

[17] 1. The DEMs of *Herrick and Sharpton* [2000] were derived from data collected during cycles 1 and 3 of the Magellan mission. These two cycles both collected

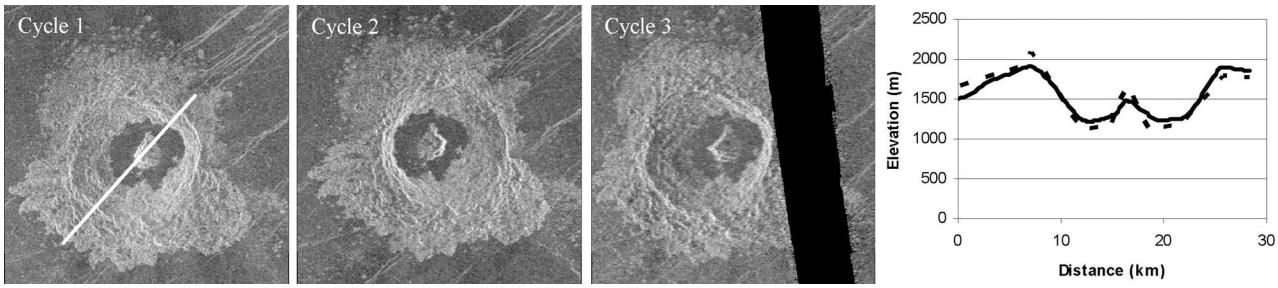

Figure 2. Ma Shouzhen crater (D = 18 km, located at 35.7°S, 92.5°E) in all three cycles of Magellan imaging. Cycle 1 and cycle 3 images were collected with the SAR looking east, while the cycle 2 image was collected with the instrument looking west. While the images are generally similar in appearance, steeper slopes such as the crater walls look very different. Note that the east crater wall is foreshortened in cycles 1 and 3, but the west crater wall is foreshortened in the cycle 2 image. Automated matching techniques work well with "same side" stereo (cycle 1 – cycle 3) pairs, but manual matching is usually necessary with "opposite look" pairs (cycle 1 – cycle 2). Graph compares profile from DEM generated from cycle 1 – cycle 3 pair (solid line) with profile produced using cycle 1 – cycle 2 pair (dashed line).

left-looking (pointing East in a North-South orbit) Synthetic Aperture Radar (SAR) data at an image resolution of ~100 m with look angles typically separated by ~20 degrees. About 20% of the planet is covered by this "left-left" stereo imagery.

[18] 2. Using a technique similar to stereo photogrammetry, topography is derived by measuring relative offsets between the locations of features identifiable in each image within a stereo pair. These match points are identified using an automated, iterative cross-correlation technique followed by manual editing.

[19] 3. Topography that was derived from the left-left stereo data and presented by *Herrick and Sharpton* [2000] has a nominal horizontal resolution of 900 m and vertical resolution of 50–100 m. Selected features, such as the crater rim, can be resolved horizontally at the image resolution. For comparison, the Magellan altimetry has a similar vertical resolution and a horizontal resolution of ~10 km.

[20] The results of *Herrick and Sharpton* [2000] spanned the full diameter range of Venusian craters and included all bright-floored craters with D > 12 km that were covered by left-left stereo imagery. In later work [*Herrick and Forsberg-Taylor*, 2003] it was determined that fresh crater depths on Venus varied substantially for D < 15 km because impactor breakup and separation caused some craters to be shallow, clustered impacts. Here we consider only craters with D > 15 km because we want to minimize impact-generated depth variations and focus on postimpact modification. We also note that using purely automated matching methodologies with left-left imagery, *Cochrane and Ghail* [2006] generated DEMs for a number of the craters presented here. Their results are mostly consistent with ours. We favor including manual editing as a processing step, as our experience indicates that the automated matching often produces artifacts in the final DEM. They confirmed the observations of impactor breakup effects for small craters. They did not explore the issue of comparing bright- and dark-floored craters.

[21] Considering only craters with D > 15 km, *Herrick and Sharpton* [2000] examined 47 craters, 21 of which have bright floors. That total includes all available bright-floored craters in the left-left coverage area, but that coverage area also contains 26 additional dark-floored craters with D > 15 km. We have now generated DEMs for all of these craters. To increase the number of bright-floored craters for which we can obtain depth data, we have to turn to the "right-left" stereo imagery. Cycle 2 of the Magellan mission collected SAR imagery for ~45% of the planet in a right-looking geometry. While this data can be combined with left-looking imagery to generate topography, its opposite look geometry makes the images in a stereo pair look different enough that automated matching techniques have minimal success (Figure 2). For craters imaged with a right-left stereo pair, we can manually generate adequate match points in order to assess rim, terrain, floor, and central structure elevations.

[22] We have thus increased our sample size for D > 15 km to 91 craters, 40 of which have a radar-bright floor. For the craters covered by left-left stereo imagery, DEM generation and data analysis are the same as *Herrick and Sharpton* [2000]. The elevations of the rim, floor, central structure, and surrounding terrain are evaluated by averaging samples from the DEM. The standard deviation of these samples is also calculated and assumed to be an estimate of the error. The four elevation values are then used to derive crater measurements such as rim-floor depth, terrain-floor depth, and so on. For right-left data, in almost all cases automatching was unsuccessful. Generally, match points were manually selected in the imagery to generate a representative profile of the crater. Based on the standard deviations of the left-left derived DEMs, we expect that these representative profiles are within ~100 m of what the crater average would be if a complete DEM could be generated. Crater locations and diameters are from *Herrick et al.* [1997]. The data for all of the craters in this study are presented the auxiliary material.[1]

[23] Figures 3–6 show rim-floor depths, rim heights, terrain-floor depths, and central structure heights, respectively. We purposely exclude two craters, Mead and Cleopatra, from these plots. Mead, at a diameter of 269 km, is more than twice the diameter of the next largest crater in the survey and is a different class of impact structure (a detailed discussion of Mead is in the work of *Herrick and Sharpton* [1996]). There are substantial mosaicking problems with Cleopatra, it is located on the side of a steeply sloping mountain, and its

[1] Auxiliary materials are available in the HTML. doi:10.1029/2010JE003722.

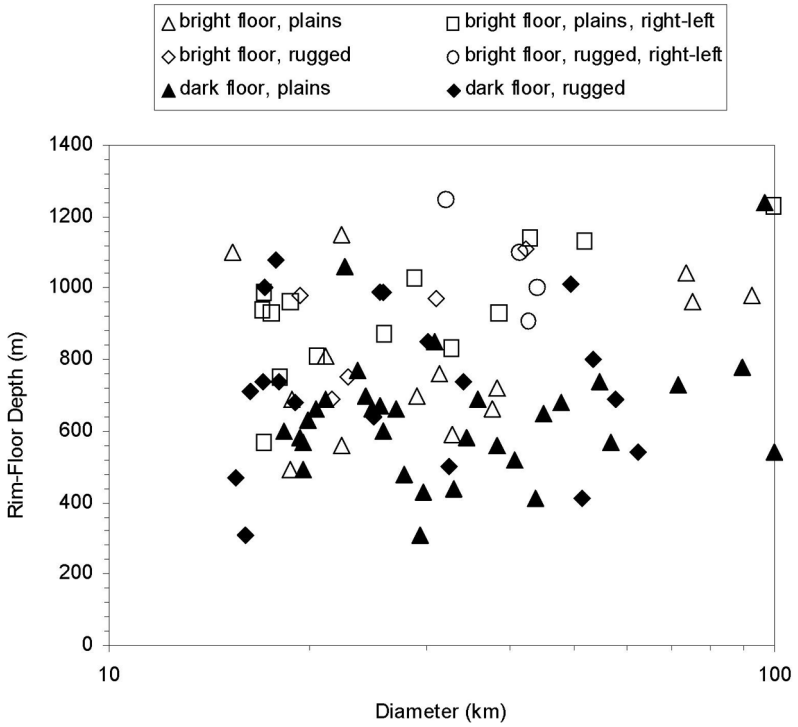

Figure 3. Rim-floor depths of Venusian craters with D > 15 km. For convenience in the plotting program, diameters of Stanton (D = 109 km) and Joliot-Curie (D = 101 km) are plotted as 100 km in this and subsequent graphs.

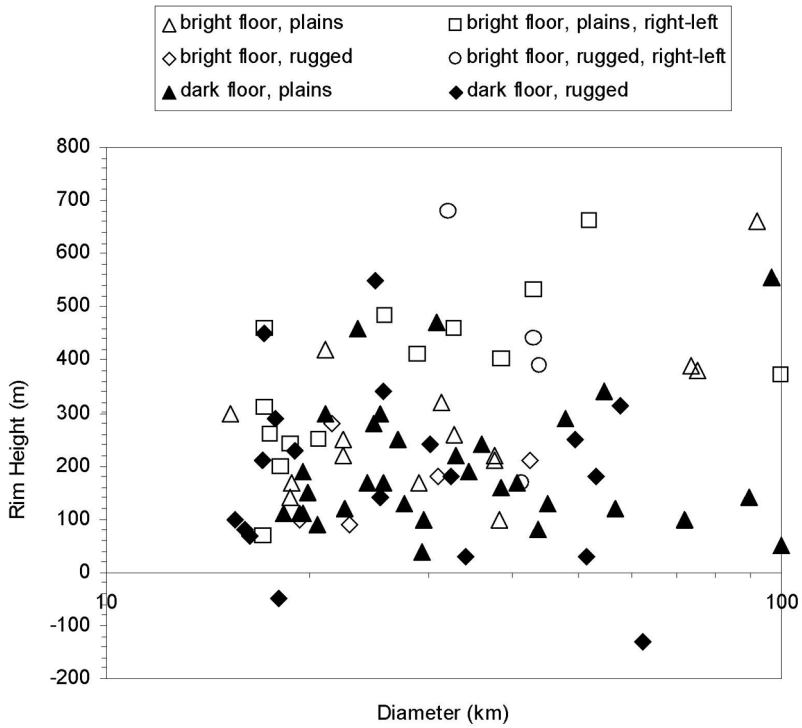

Figure 4. Rim heights of Venusian craters with D > 15 km. Because terrain height is calculated by fitting a plane to points surrounding the crater, for two craters in very rugged terrain the calculated rim height is artificially negative.

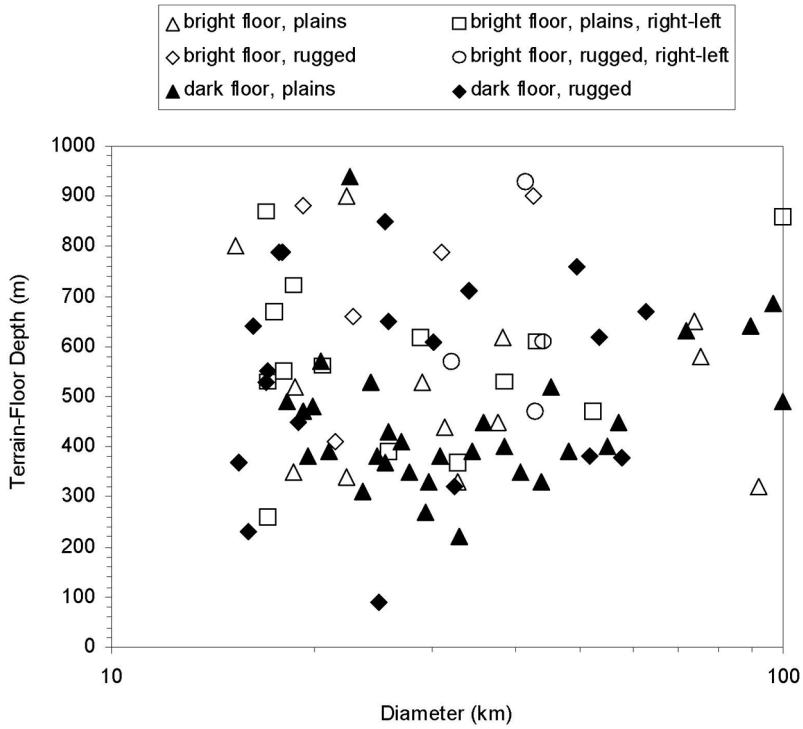

Figure 5. Terrain-floor depths of Venusian craters with D > 15 km.

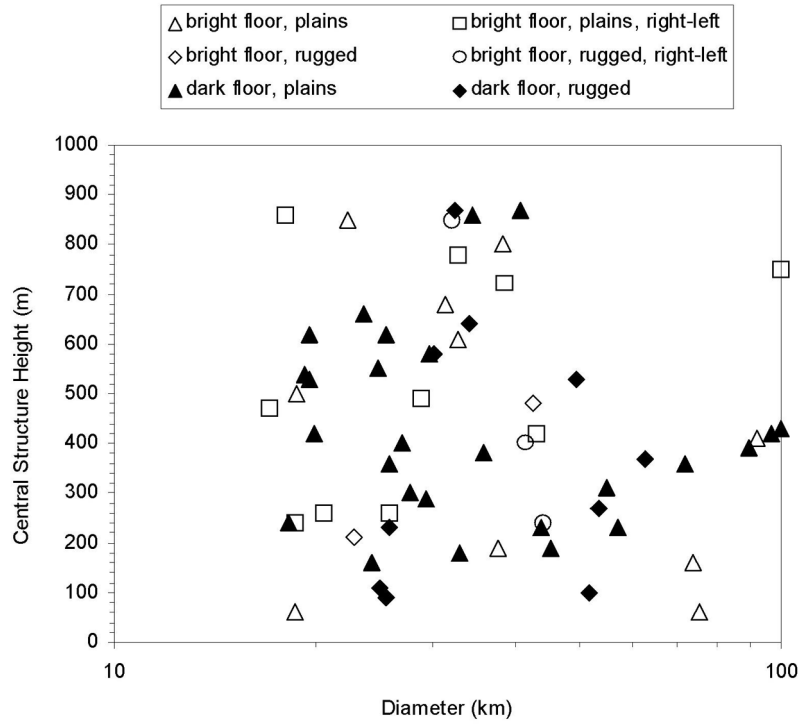

Figure 6. Elevations of central structure relative to crater floor for Venusian craters with D > 15 km.

Table 1. Best Fit Trends for Rim-Floor Depths, Rim Heights, Terrain-Floor Depths, and Central Structure Heights for Craters with D > 15 km[a]

						Values of Trends (m)	
	n	*b*	SD *b*	*A*	SD *A*	D = 30 km	D = 90 km
				Rim-Floor Depths			
Bright floors (plains)	28	0.165	0.082	0.483	0.137	847	1016
Bright floors (all)	37	0.186	0.074	0.462	0.118	870	1068
Dark floors (plains)	32	0.108	0.097	0.424	0.149	612	689
All craters in survey	88	0.0917	0.0667	0.536	0.124	732	809
				Rim Heights			
Bright floors (plains)	29	0.483	0.189	0.0558	0.0382	289	491
Dark floors (plains)	32	−0.0247	0.228	0.181	0.162	167	162
All craters in survey	89	0.114	0.227	0.123	0.107	182	206
				Terrain-Floor Depths			
Bright floors (plains)	28	0.00445	0.1183	0.509	0.212	517	520
Dark floors (plains)	32	0.141	0.102	0.260	0.0961	420	490
All craters in survey	88	0.0575	0.084	0.402	0.118	489	520
				Central Structure Heights			
Bright floors (plains)	20	−0.139	0.341	0.617	0.941	384	330
Dark floors (plains)	26	−0.126	0.182	0.604	0.422	393	343
All craters in survey	61	−0.0879	0.177	0.499	0.337	370	336

[a]All fits of form $y = A*D^b$, where D is diameter, and y and D are in kilometers. Fits were performed in log-log space. Standard deviation is "SD," and n is number of craters used in calculating the trend.

interior structure is unusual. Thus, we cannot obtain representative values for the rim, floor, surrounding terrain, or central structure.

[24] We show separate symbols for craters located on volcanic plains, a flat target, versus those in more rugged terrains where preexisting topography might have affected final crater shape. We also identify those craters with parameters estimated from the right-left stereo data. Trends for the data are summarized in Table 1, where data have been linearly fit in log-log space to an exponential function. The data show an obvious difference in rim-floor depths and rim heights between bright- and dark-floored craters. As in the work of *Herrick and Sharpton* [2000], the trends for rim-floor depths and rim heights are separated by more than the error associated with them. Terrain-floor depths are similar between the two populations. In Table 2 we normalize the measurements by the best fit trend for bright-floored craters in the plains, and then we compare the data sets using a Fisher-Behrens test. We find that the mean normalized values of dark-floored and bright-floored craters are different at the 99% confidence level for rim-floor depths and rim heights, but the populations for terrain-floor depths are not significantly different.

[25] The data for central structure heights should be taken with a large grain of salt, as these features often have significant layover in the imagery. The most notable feature of central structure heights is their large variability. Central peaks and peak rings range from minimal structures with negligible elevation to structures that rise above the rim. With limited data, *Herrick and Sharpton* [2000] plotted the difference in elevation between the top of the central structure and the crater rim, and their limited data suggested a bimodal distribution. However, the same plot with more data (Figure 7) shows only a large scatter.

[26] In summary, our results reaffirm the conclusion of *Herrick and Sharpton* [2000] that dark-floored craters have, on average, experienced significant amounts of postimpact volcanism both interior and exterior to the crater. Since ~80% of Venusian impact craters have radar-dark floors [*Herrick and Phillips*, 1994], this implies significant and widespread volcanism (at least a few hundred meters, globally averaged) during the time period that the crater population was emplaced.

3. Dark Halos Around Impact Structures

[27] Halos of relatively low backscatter are found around roughly one third of Venusian craters, and they extend 3–4 crater radii beyond the ejecta blanket [*Phillips et al.*, 1991;

Table 2. Fisher-Behrens Tests of Population for Rim-Floor Heights, Rim Heights, and Terrain-Floor Heights for Dark-Floored Versus Bright-Floored Craters As in the Work of *Herrick and Sharpton* [2000][a]

	n	Mean	Variance
	Rim-Floor Depths		
Bright floors (plains)	28	1.02	0.050
Dark floors (plains)	32	0.74	0.038
Degrees of freedom: 56			
t statistic: 5.14			
	Rim Heights		
Bright floors (plains)	29	1.09	0.204
Dark floors (plains)	32	0.66	0.159
Degrees of freedom: 58			
t statistic: 3.92			
	Terrain-Floor Depths		
Bright floors (plains)	28	1.05	0.116
Dark floors (plains)	32	0.86	0.071
Degrees of freedom: 53			
t statistic: 2.44			

[a]For each measurement type, the values are normalized to the best fit trend for bright-floored craters in the plains, and then the two sample populations are compared. Values above 2.7 for the *t* statistic indicate a significant difference in the two sample populations at a 99% confidence level. See *Johnson* [1973] for summary of Fisher-Behrens test. The number of craters in the sample is *n*.

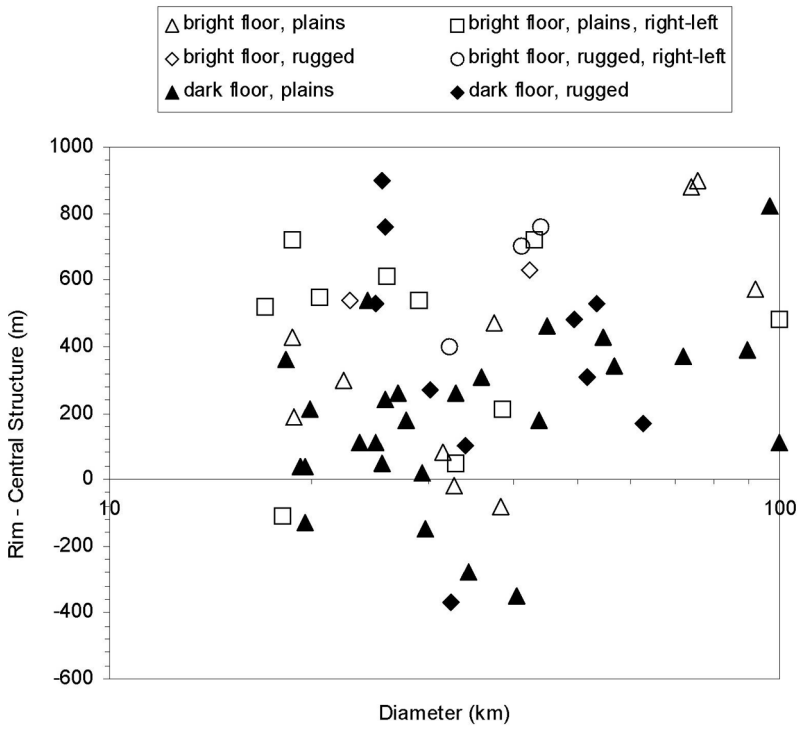

Figure 7. Difference in elevation between the rim and the top of the central structure for Venusian craters with D > 15 km.

Herrick and Phillips, 1994]. The most common explanation for their origin is comminution, and thus smoothing, of the surface by a downgoing projectile-generated atmospheric shock wave [*Phillips et al.*, 1991], although some dark halos have sharp margins and potential flow features that suggest origin by flow of fine-grained ejecta [*Schultz*, 1992]. Both hypotheses indicate that dark halos form at the time of impact, so their apparent presence around many dark-floored craters casts doubt on the conclusion that those craters have probably experienced embayment by external volcanism. A possible solution to this conundrum is that regional volcanism covers the floor and portions of the crater exterior without completely eliminating the dark halo. The crater and associated deposits for even a moderate-sized, 20 km diameter structure can cover several thousand square kilometers, so it seems reasonable that regional volcanism could cover significant portions of a crater structure but leave other areas intact.

[28] We examined all of the craters with D > 20 km diameter that *Herrick et al.* [1997] classified as having a dark halo (~1/3 of the craters in that size range). We evaluated whether or not the dark halo completely surrounded the crater. More specifically, we assessed whether there is a continuous area of relatively low backscatter beyond the entire perimeter of the terminus of the rim and radar-bright ejecta. Similarly we assessed whether radar-bright ejecta could be found all the way around the crater rim. If regional volcanism is responsible for dark floors, then complete halos should occur only with bright-floored craters. As Table 3 shows, only a small fraction (7 of 114 craters) has an apparently complete dark halo and a dark floor. Those craters are Hwangcini (6.3 N, 141.7 E, D = 31 km), Lind (50.2 N, 355.0 E, D = 25 km), Polina (42.4 N, 148.2 E, D = 21 km), Barton (27.4 N, 337.5 E, D = 50 km), Danilova (26.4 S, 337.2 E, D = 48 km), Orczy (3.7 N, 52.3 E, D = 27 km), and Buck (5.7 S, 349.6 E, D = 22 km). Of those seven craters, for three of the craters (Hwangcini, Barton, Orczy), a regional view suggests that the apparent dark halo may be part of a larger area of radar-dark plains (Figure 8). For Barton, it is possible that the nearby crater Lachappelle (26.7 N, 336.7 E, D = 35 km) occurred later, and remnants of its parabolic feature are blanketing the floor of Barton and created some or all of what is perceived as a dark halo (Figure 9). This scenario is consistent with the interpretation by *Carter et al.* [2004] that Arecibo polarization data shows an extensive crater-derived mantling deposit in the region. For five of the seven craters there are small volcanic edifices in close proximity to the crater (Hwangcini, Polina, Barton, Danilova, Orczy), and it may be that minor volcanism is generating the dark floor without affecting the halo (Figures 8 and 9). Nevertheless, there are a few craters, such as Buck (Figure 10), that are potentially inconsistent with the regional

Table 3. Survey of Craters With D > 20 km and a Radar-Dark Halo[a]

Complete Halo	Bright Floor	Surrounding Ejecta	Number
y	n	y	3
y	n	n	4
y	y	y	21
y	y	n	9
n	n	n	50
n	y	n	9
n	n	y	14
n	y	y	4
		Total	114

[a]Columns indicate how many craters had a complete dark halo, bright floor, and ejecta completely surrounding rim.

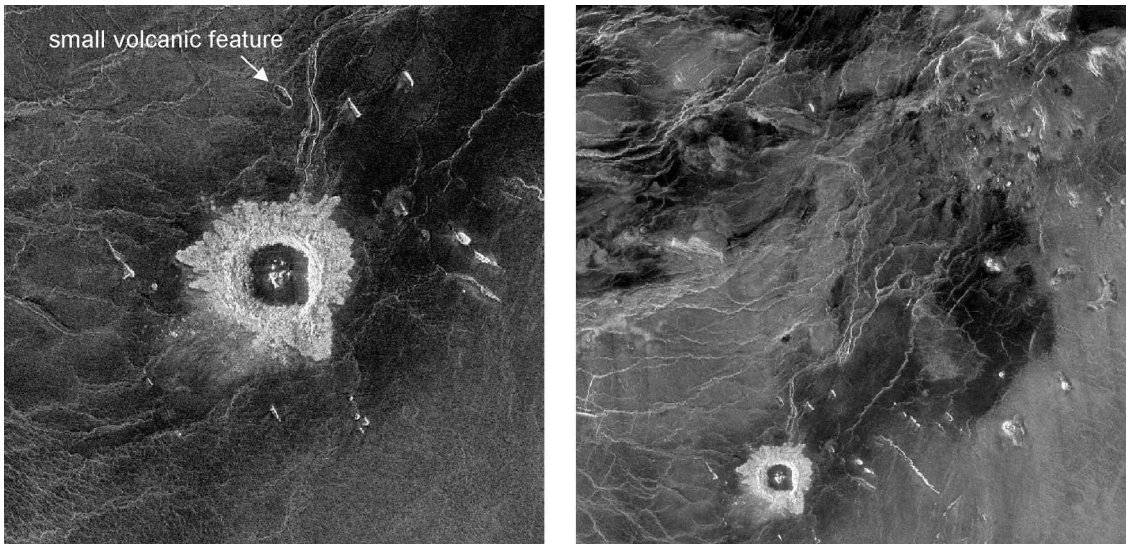

Figure 8. (left) Local and (right) regional view of crater Orczy (3.7°N, 52.3°E, D = 27 km), one of a few craters with a complete dark halo and a dark floor. The local view shows abundant small volcanic features in the vicinity of the crater (one of many examples shown by arrow), which suggests that perhaps unseen vents may have caused volcanic flooding of the crater floor. The regional view suggests that the dark halo may not be related to the crater at all, but simply part of a larger regional radar-dark area. Regional view spans from 51.7 to 54.7°E, and 3.2 to 6.7°N.

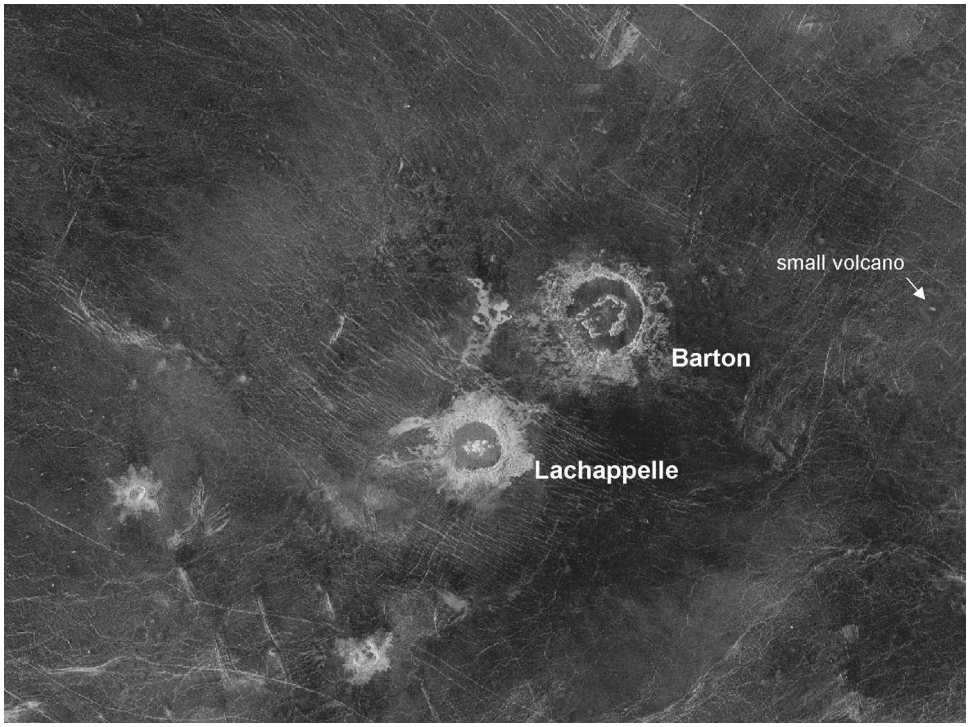

Figure 9. The dark halo surrounding Barton (27.4°N, 337.5°E, D = 50 km) and its dark floor may both be mantling deposits from the remnants of a large parabolic feature associated with the nearby, brighter-floored crater Lachappelle (D = 35 km). Note that there are also a number of small volcanic features in the area (white dots indicate the summit pits; arrow points to one of many examples). View spans from 334 to 339.8°E, and 25.2 to 29.0°N.

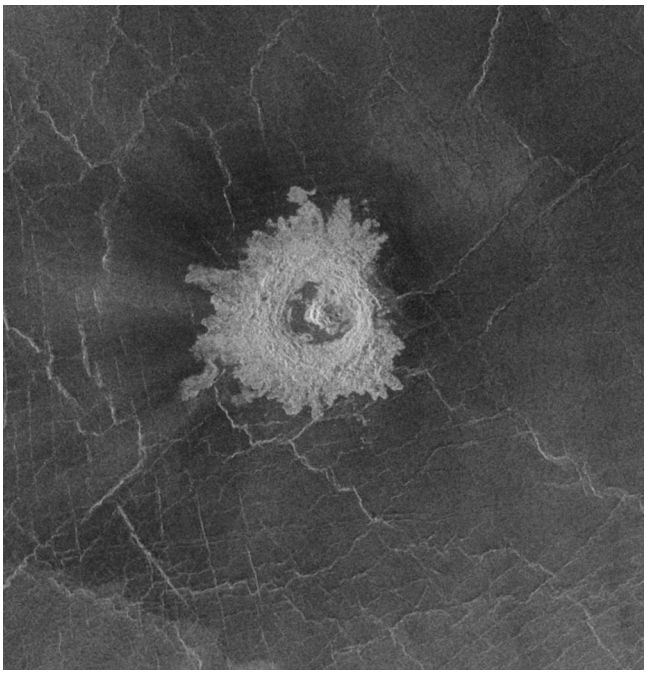

Figure 10. Impact crater Buck (3.7°N, 52.3°E, D = 27 km), an isolated impact crater in the plains with an intact dark halo and a floor with similar backscatter properties to the surrounding terrain.

volcanism hypothesis for dark-floored craters. These craters either formed with a radar-dark floor, experienced in situ weathering of an initially bright floor [*Arvidson et al.*, 1992], or experienced postimpact volcanism confined to the crater interior.

[29] While oblique impact produces minimal ejecta on the uprange side of the crater, a lack of ejecta all the way to rim may be an indicator of exterior embayment to the rim [*Herrick and Forsberg-Taylor*, 2003]. Consistent with this view, the majority of craters with a complete halo and/or a bright floor have ejecta surrounding the entire rim, and most of the craters with a dark floor and/or less than a complete dark halo have a portion of the rim with no adjacent ejecta.

[30] We note that *Basilevsky and Head* [2002b] generated their own database of dark halo deposits for craters with D > 30 km. They identified more craters with haloes than *Herrick et al.* [1997], and they state that most of these additions were craters with partial haloes or haloes not directly connected to the crater. Consequently, including their additional craters would not alter our interpretation of the data.

[31] In summary, the dark halo data are, with perhaps a few exceptions, consistent with the scenario that dark-floored craters are structures that have experienced both internal and external volcanic embayment. Almost all dark halo craters that have dark floors have only partial halos, and it is feasible that the halo remains intact in some areas even though the ejecta and floor have experienced some volcanic filling and embayment.

4. Detailed Histories of Large Impact Structures

[32] Sections 2 and 3 provided statistical evidence, supported by qualitative observations, that most Venusian impact craters have experienced some postimpact volcanic modification. In this section we evaluate the geologic histories of the largest impact craters to gain insight into the nature of crater modification processes. Previous work illustrated that Mead, the largest impact basin on Venus with a diameter of 269 km, has experienced viscous relaxation of the floor and volcanic flooding of the ejecta and outer ring [*Herrick and Sharpton*, 1996]. Here we evaluate all the remaining impact structures on Venus that have significant left-left stereo coverage and are over 45 km in diameter. Figure 11 shows the locations of these structures and Table 4 summarizes their properties. We use standard photogeologic techniques aided by the stereo-derived topography. In cases where previous authors have analyzed the geology of the region that includes the crater, we discuss the consistency of our results with theirs. We present the histories of the craters in order of decreasing crater diameter.

4.1. Cleopatra, Latitude 65.9°N, Longitude 7.0°E, Diameter 105 km

[33] By virtue of its large diameter and location on the eastern slope of Maxwell Montes, Cleopatra is one of the more prominent geologic features on the surface of Venus (Figure 12). The structure was first clearly imaged by the Venera orbiters in the mid-1980s. *Ivanov et al.* [1986] described many of the basic features of the crater. Cleopatra has an interior peak ring that is ~50 km in diameter, consistent with a 2:1 ratio of crater diameter to peak ring diameter for peak ring craters on the terrestrial planets. The terrain surrounding Cleopatra is smoother in Venera imagery than the remainder of Maxwell Montes, and *Ivanov et al.* [1986] interpreted this as mantling by ejecta. The peak ring is offset to the west-northwest relative to the crater center. The rim is subdued and is not significantly elevated above the surrounding terrain. *Schaber et al.* [1986] noted a breach in the rim that seemed to lead downslope to a volcanic deposit, and this was the main observation that led them to an interpretation of Cleopatra as a volcanic caldera. In a later pre-Magellan discussion of Cleopatra, *Basilevsky and Ivanov* [1990] noted that the depth of Cleopatra is over 2 km. After Magellan returned imagery of Cleopatra, *Basilevsky and Schaber* [1991] reexamined Cleopatra and concluded that it was definitely an impact structure. Except as noted, our observations and interpretation do not differ substantively from theirs.

[34] The steep slopes of Maxwell Montes caused some obvious artifacts in both the gridded altimetry data (the Global Topographic Data Record, or GTDR) and the stereo-derived topography that we show in Figure 13. However, the data is adequate to make some key observations. Our data confirm that the rim has little or no elevation relative to the surrounding terrain, and consequently the rim varies in elevation by ~1 km from west to east as it follows the general slope of Maxwell Montes. The crater floor exterior to the peak ring appears to be flat at a constant elevation that ranges from ~500–1500 m below the crater rim. Inside the peak ring, the topography sags by another kilometer, so that the crater center is up to 2.5 km lower than the crater rim. There is no indication of tectonic tilting of the crater floor, and we could find no evidence of postimpact tectonic deformation within the crater.

[35] The crater floor exterior to the peak ring is lower in backscatter than the mountainous terrain surrounding the rim,

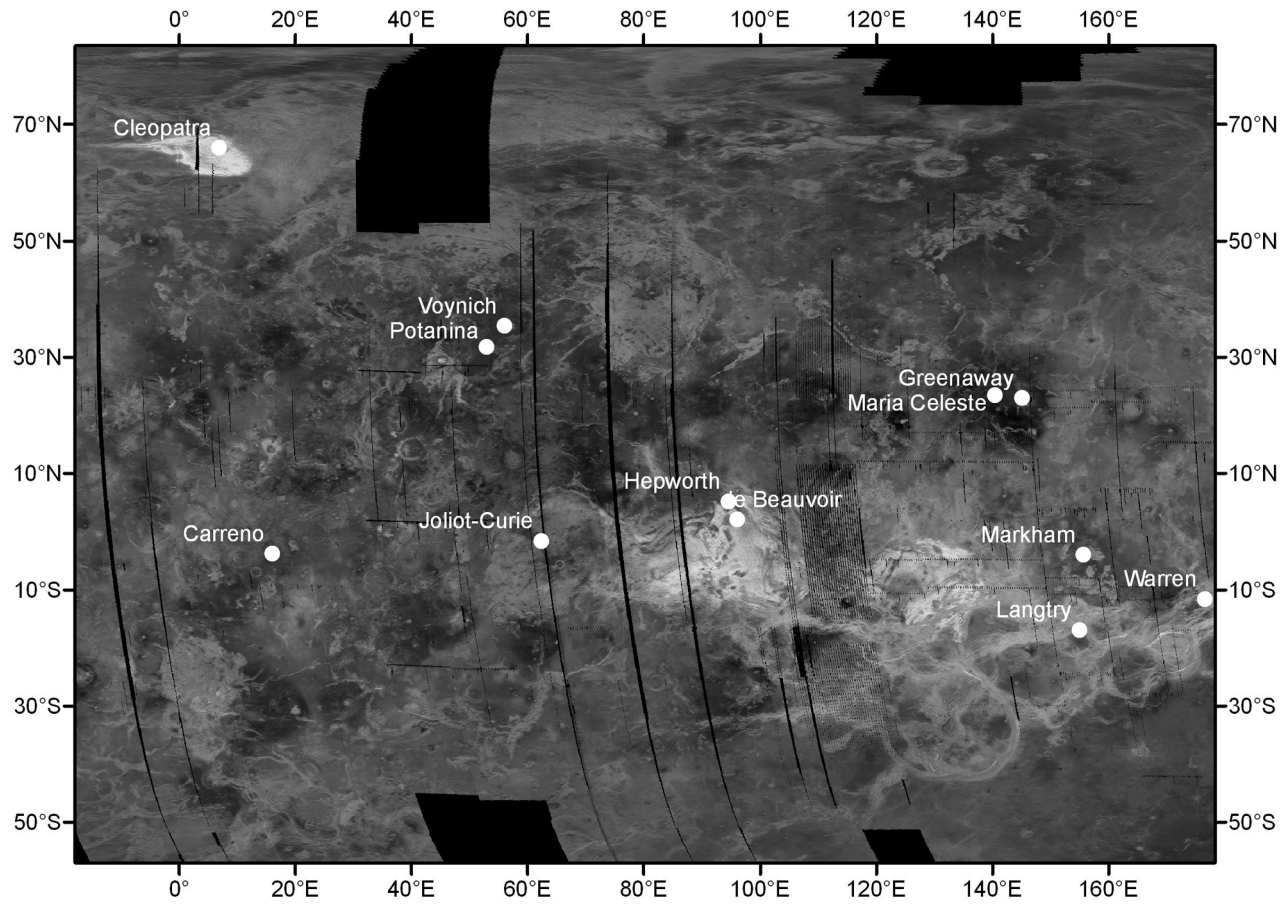

Figure 11. Locations of the craters we studied for their geologic histories.

and the surface is even darker inside the peak ring (Figure 14). The inner area's relatively low backscatter may be partially due to it being below the regional "snow line," a planetary radius of ~6056.0 km above which there is a marked increase in the reflectivity of the surface material of Maxwell Montes. However, in the southern part of the area inside the peak ring there appear to be sharp geologic (not related to elevation) contacts between the low-backscatter material of the inner area and the higher-backscatter materials of the outer area. We conclude that the material inside the peak ring must be compositionally or texturally different from material exterior to the ring.

[36] From within the peak ring there is a low-backscatter drainage channel that goes through the peak ring, crosses the crater floor, and cuts through a low area in the crater rim. Material has drained from inside the peak ring through the

Table 4. Summary of Large Impact Structures That We Studied in Detail

Name	Latitude	Longitude	Diameter (km)	Rim-Floor Depth (m)	Rim Height (m)	Surrounding Terrain	Postimpact[a]
Cleopatra	65.9	7.0	105	500–1500[b]	~0[b]	Maxwell Montes	-
Joliot-Curie	−1.7	62.4	101	540	50	tessera and plains	V, T
Maria Celeste	23.4	140.4	97	1240	555	plains	mV
Greenaway	22.9	145.1	92	980	660	plains	V
Potanina	31.7	53.0	90	780	140	volcanic flows	V
Markham	−4.1	155.6	72	730	100	plains and coronae	V, T
Hepworth	5.1	94.6	63	540	~0[c]	tessera and plains	MV, MT
Carreno	−3.9	16.1	57	570	120	plains	mV, mT
de Beauvoir	2.0	96.1	53	800	180	tessera	V, T
Langtry	−17.0	155.0	52	410	30	rift	V, T
Warren	−11.7	176.5	49	1010	250	rift	MV, MT
Voynich	35.3	56.1	48	680	290	plains	V

[a]"V" indicates that postimpact volcanism embays or floods the crater, "T" indicates tectonic deformation, "M" indicates multiple episodes of volcanism or deformation, and "m" indicates minor activity.
[b]Topography of Cleopatra's rim is highly variable and apparently not elevated relative to the surrounding terrain.
[c]Variations in the surrounding terrain elevation resulted in a physically impossible negative rim height from the methodology we used.

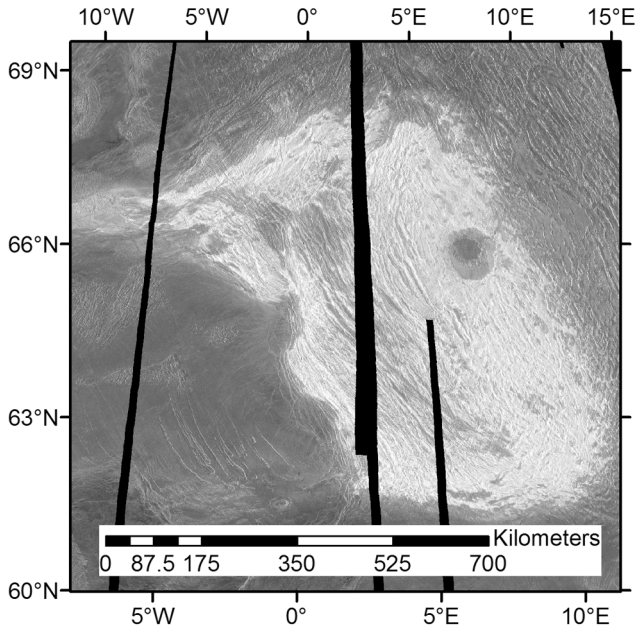

Figure 12. Regional image showing Cleopatra (65.9°N, 7.0°E, D = 105 km) located on the northeast slope of Maxwell Montes.

channel, and continued to form a topographically smooth deposit downslope from the crater. *Basilevsky and Schaber* [1991] interpreted this deposit to have resulted from impact-triggered volcanism. Given a lack of obvious volcanic features within Cleopatra, and little evidence of postimpact modification, we favor an interpretation that the channel drained impact melt. In this view, immediately after crater formation, impact melt contained within the peak ring was at a higher hydrostatic level than material exterior to the peak ring. A breach of the peak ring and fortuitous surface topography allowed the material to drain out the northeast rim of the crater. Later thermal subsidence caused significant depression of the crater floor inside the peak ring.

[37] Overall, we are driven to the conclusion that Cleopatra is an impact structure that has not been significantly altered since formation. This interpretation is based on the lack of evidence for postimpact interior faulting and the preservation of the different terrains inside and outside the peak ring. However, in full-resolution Magellan imagery there are only a few places around the rim where unambiguous ejecta deposits cover the surrounding terrain, and there is no obvious topographic expression for the crater rim. If Cleopatra is a pristine crater, it is certainly an unusual one.

4.2. Joliot-Curie, Latitude 1.7°S, Longitude 62.4°E, Diameter 101 km

[38] Joliot-Curie is located in the westernmost portion of Aphrodite Terra in Manatum Tessera. The crater is on a regional topographic low in the tessera and straddles an area of volcanic plains that extends to Verdandi Corona to the southeast and Disani Corona to the northwest. Figure 15 shows a stereo anaglyph of the crater that indicates the extent of stereo coverage. The southwestern ejecta appears to superpose the tessera and volcanic plains. The rim has little elevation relative to the plains to the south, so it may be that some postcrater embayment of the tessera and ejecta has occurred there.

[39] The eastern half of the crater, which unfortunately does not have stereo coverage, does not appear to be pristine. The ejecta north of the crater and adjacent to the eastern rim of the crater are present on high-standing tessera but not on the low-lying radar-dark plains that appear to partially flood the tessera (Figure 16). This clearly indicates that the northern and eastern ejecta of the crater have been partially covered by postimpact lavas.

[40] The eastern tessera deformation appears to deform the rim of the crater. Joliot-Curie also has a nonsymmetric peak ring, and the southeastern portion of the ring has a tessera-like fabric (Figure 17). The peak ring is particularly unusual when one considers that Cleopatra crater has a symmetric peak ring without a tessera-like appearance. We suggest that significant deformation of the eastern half of the crater occurred. The amount of deformation is not great enough to make the crater noncircular, but is enough to distort the appearance of the eastern rim and inner ring; this could be accomplished with strains on the order of 1%. Subsequent volcanism then covered the deformation of the crater floor and partially buried the external ejecta. Joliot-Curie has a near-zero rim height and a rim-floor depth that is ~500 m less than similar-sized bright-floored craters, indicative of several hundred meters of postimpact filling and embayment. We conclude that significant tectonic deformation and volcanism both predate and postdate Joliot-Curie.

4.3. Maria Celeste, Latitude 23.4°N, Longitude 140.4°E, Diameter 97 km

[41] Maria Celeste is an unusual peak ring structure located in the volcanic plains northeast of Thetis Regio in Llorona Planitia (Figure 18). This overall region of plains has a low backscatter resulting from mantling by dark parabolas associated with the craters Greenaway, ~450 km to the east, and Ban Zhao, ~900 km to the southeast. Maria Celeste is located within the dark parabola associated with Greenaway [*Campbell et al.*, 1992]. *Schultz* [1992] identified the structure as an oblique impact with the projectile direction of travel to the northwest. There is a "forbidden zone" to the southeast that lacks ejecta. The ejecta appears to have been swept to the northwest by impact-generated winds. *Schultz* [1992] interpreted the obvious northwest offset of the peak ring relative to crater center as resulting primarily from enhanced uprange rimwall failure. He interpreted the rectilinear fault pattern on the uprange rim as faulting of an oversteepened rim wall that was controlled by the regional tectonic fabric.

[42] The limited stereo coverage (Figure 18) was adequate to allow assessment of depth and rim height, but several key areas within and surrounding the crater are not covered. The rim-floor depth (1240 m) and rim height (560 m) are fairly high and consistent with those for fresh, bright-floored craters. As with Cleopatra, the area inside the peak ring is lower in backscatter than the area exterior to the peak ring, and the low-backscatter material clearly embays material associated with the peak ring. The edges of this inner, low-backscatter area are not substantially lower than the brighter material outside the peak ring, but topography sags to the center by ~200 m.

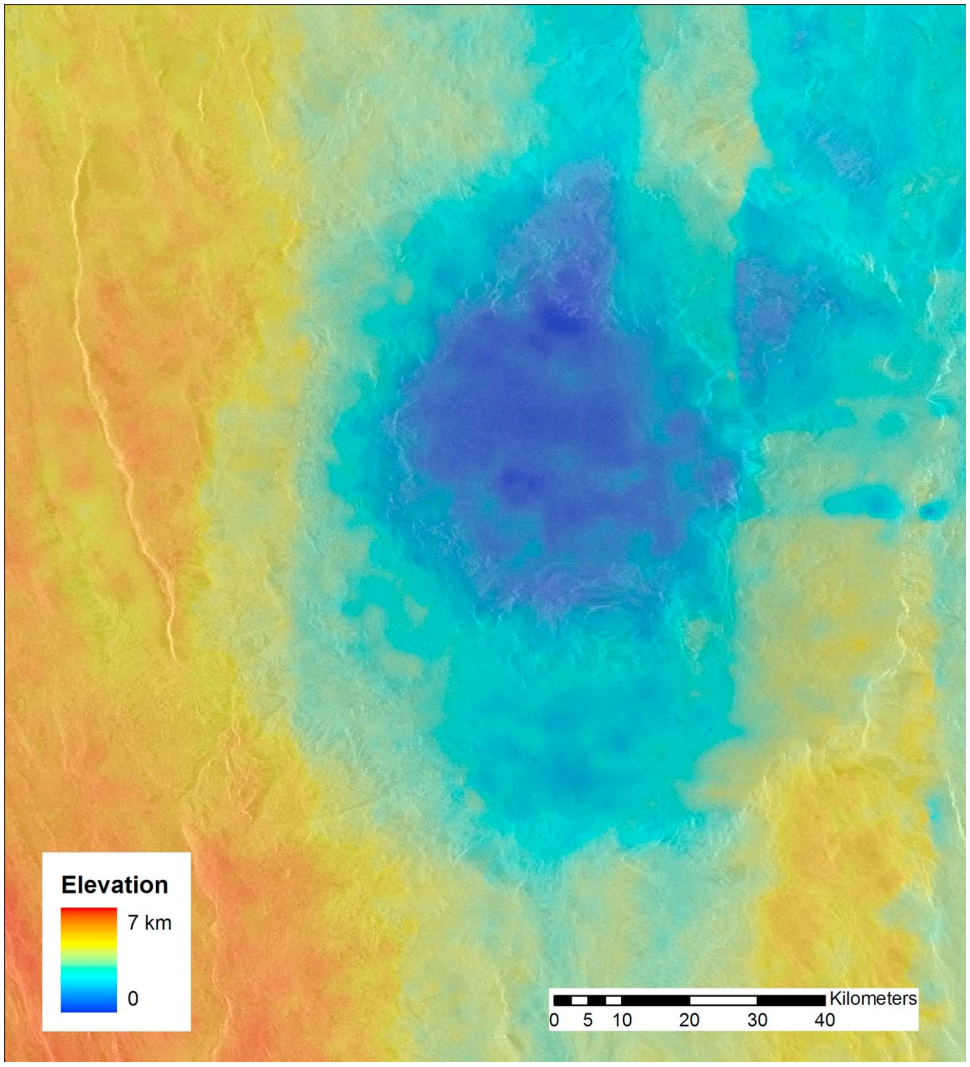

Figure 13. Stereo-derived topography of Cleopatra superposed on orthorectified cycle 1 image. Note that mosaicking errors in the images have directly resulted in unnatural step functions in the topography.

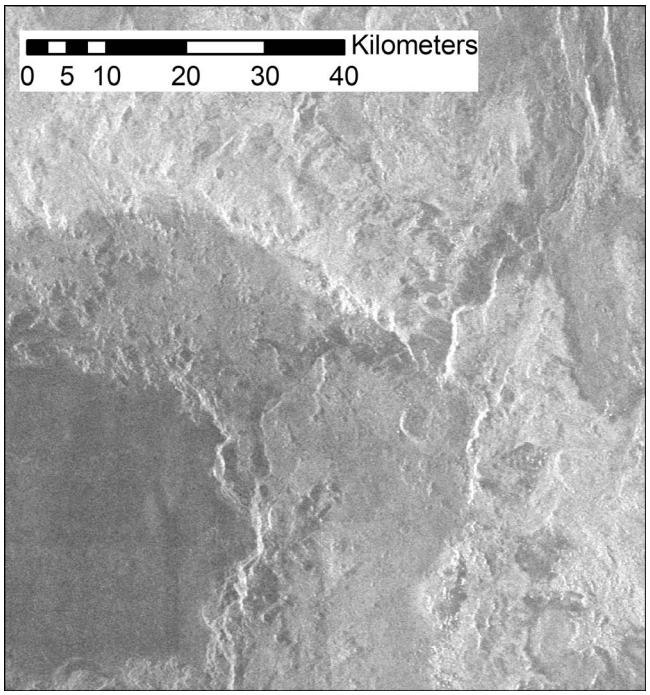

Figure 14. Cycle 1 imagery of the northeast portion of Cleopatra showing a channel that drains material from inside the peak ring to the northeast slopes of Maxwell Montes.

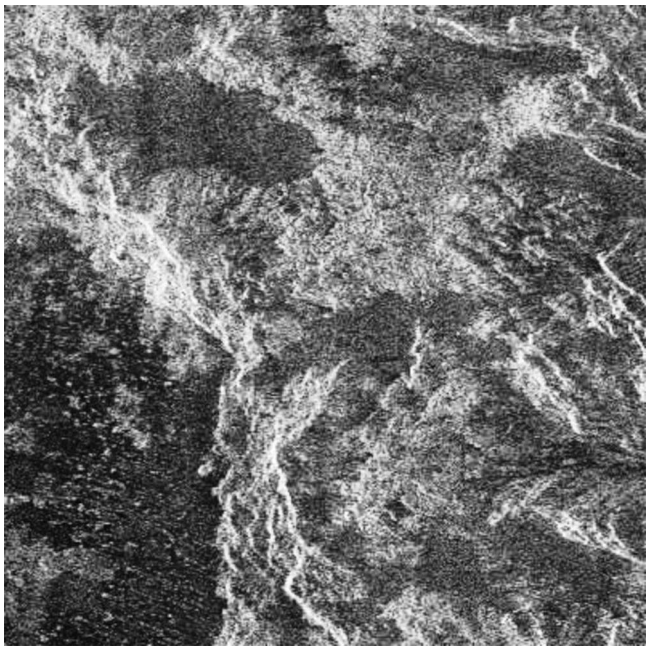

Figure 16. A 60 × 60 km image showing the northeast corner of Joliot-Curie. Ejecta appears to be only in high-standing areas exterior to the crater, and the rim appears to have experienced some postcrater deformation.

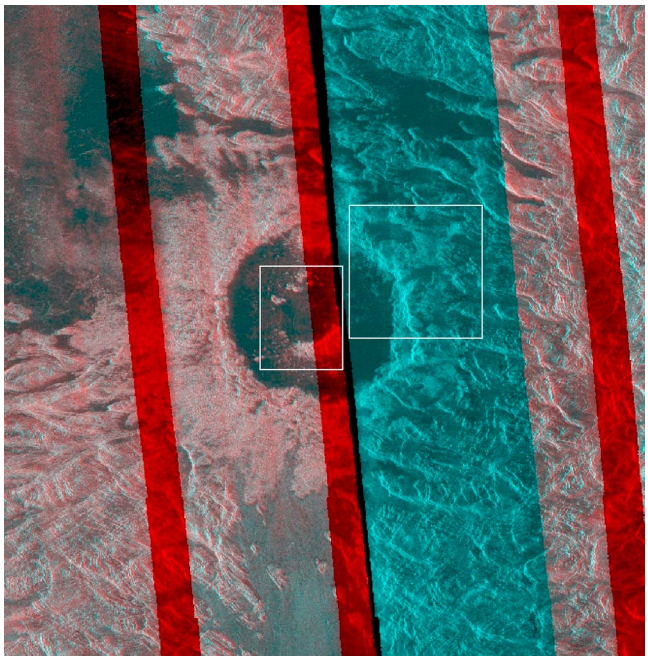

Figure 15. Stereo anaglyph of crater Joliot-Curie (1.7°S, 62.4°E, D = 101 km). Stereo coverage exists only where both red and green-blue channels are present. Note that to the southwest the ejecta appears to superpose the plains and the tessera. Boxes indicate areas shown in Figures 16 and 17.

Figure 17. This 37.5 × 40 km image illustrates the unusual nature of the southern portion of Joliot-Curie's peak ring. We interpret the ring to have experienced postimpact deformation.

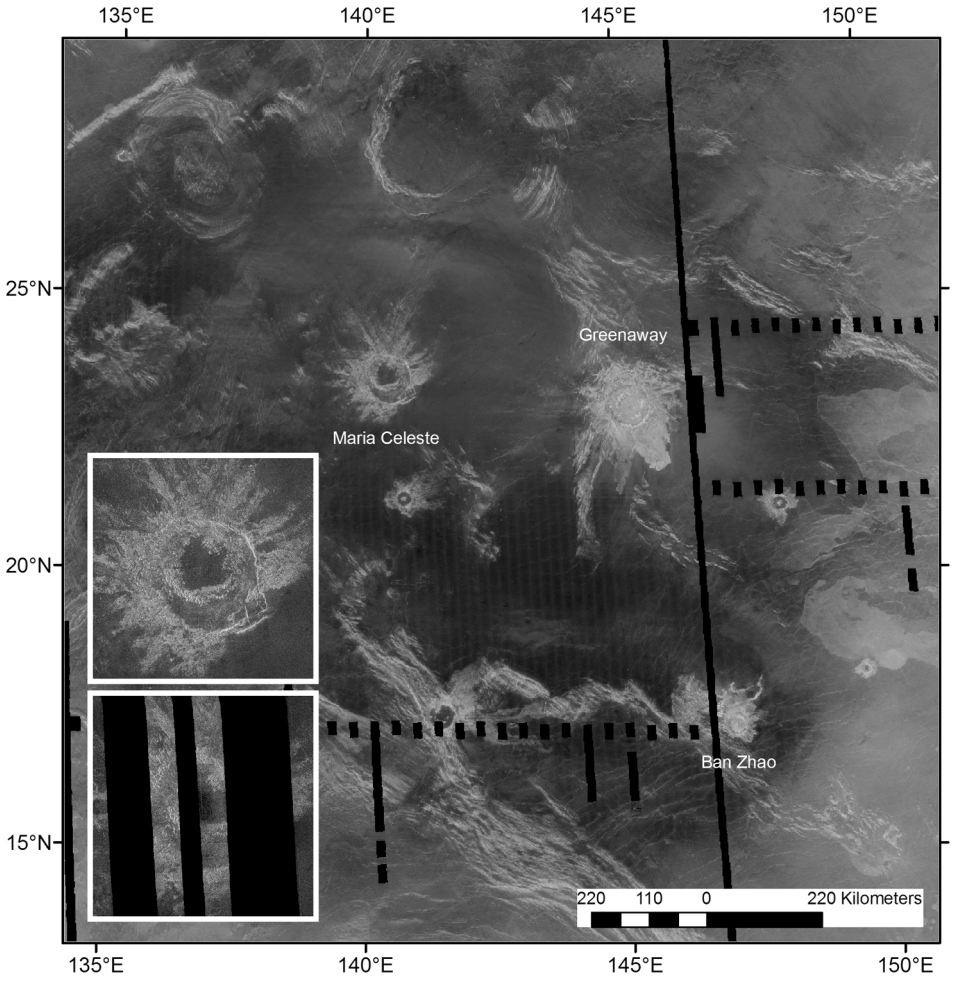

Figure 18. Regional image that shows Maria Celeste along with Greenaway and Ban Zhao. Insets show minimal stereo coverage of Maria Celeste.

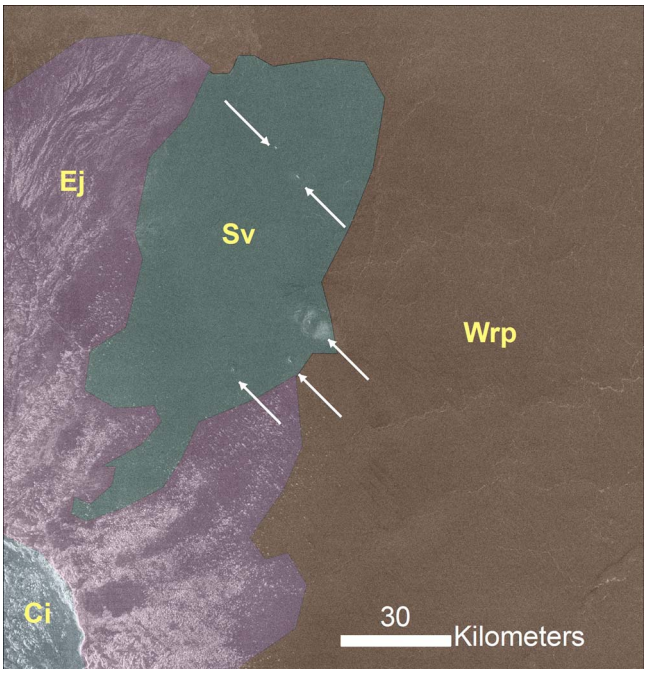

Figure 19. Close-up of area northeast of Maria Celeste's rim. Arrows indicate small volcanic structures whose flow units (Sv) superpose crater ejecta (Ej) and wrinkle ridges of surrounding plains (Wrp). Ci unit is interior of Maria Celeste.

[43] To the west the crater and its associated ejecta appear to superpose wrinkle ridges and other structures associated with the regional plains. Northeast of the crater are some small volcanic constructs. Despite the lack of well-defined flow edges, it is clear that radar-dark areas associated with these features both truncate ejecta and superpose the regional wrinkle ridge pattern (Figure 19). Similar relationships also occur south of the crater.

[44] We infer that Maria Celeste formed largely after formation and deformation of the regional volcanic plains. Portions of the ejecta blanket appear to be superposed, especially to the northeast and south, by flows associated with small volcanic features in the plains. The areal extent and the nature of features covered suggest flows with combined thickness of tens of meters. The area inside the peak ring appears to have subsided since impact formation. This area either contained impact melt of a different backscatter than material exterior to the peak ring, or there was minor volcanic flooding of this inner area. The crater and its surroundings were later mantled by deposits associated with the formation of Greenaway crater.

4.4. Greenaway, Latitude 22.9°N, Longitude 145.1°E, Diameter 92 km

[45] Greenaway is a peak ring structure located in volcanic plains ~450 km east of Maria Celeste. It has a radar-bright floor and significant ejecta flows to the south and southeast. There are a number of other impact structures in the area, and one of them, Ban Zhao, may have distal deposits that are responsible for radar darkening the southern ejecta flows of Greenaway (Figure 20). There are high-standing remnants of a ridge corona belt that has been subsequently embayed by plains volcanism to the north, southwest, and south of the crater. The crater and ejecta are superposed on this belt.

[46] The topography of the crater and its surroundings are particularly unusual (Figure 21). There is a 400–500 m drop in elevation from northwest to southeast over ~150 km in the terrain on which the crater is superposed. The flows from the crater go in the direction of this slope, and the northwest crater rim is higher than the southeast rim by a similar amount. The regional topography, including the wrinkle ridges in the plains, controls the direction of the ejecta flows in the south and southeast. The northwestern portion of the peak ring is elevated well above the floor but the southeastern portion is mostly submerged. The floor of the crater is bright, at constant elevation in the stereo-derived topography, and shows no indication of subsequent embayment. We conclude that the regional slope caused an asymmetry in the rim and peak ring elevations, while the melt on the floor assumed a hydrostatic level. The unique circumstances surrounding Greenaway's formation have some interesting implications for cratering mechanics. That the rim and peak ring parallel the regional topography suggests that the regional pressure field controlled the excavation and modification stages. However, the melt within the crater flowed to match the local geoid.

[47] We note that a data gap in the cycle 3 imagery precludes performing radargrammetry in the very center portion of the crater. The Magellan altimetry data show a depression in this region of ~150 m that has been interpreted as thermal contraction of a melt sheet that is thickest in the crater center [*Brown and Grimm*, 1996]. That interpretation is consistent with our work.

[48] While the interior of Greenaway appears to be unaffected by any postimpact volcanic processes, portions of the ejecta blanket have been embayed by later flows. On the northern edge of the ejecta there are a number of low-lying, radar-dark patches that indicate embayment (Figure 22), and in some cases small volcanic edifices are visible as the likely source. Although we do not have high-resolution topography to the west and northwest of the crater rim, our interpretation of the imagery is that postimpact plains volcanism embays part of the ejecta blanket here as well. To the southwest of the crater the stratigraphic relationships are more ambiguous, but it appears that the wrinkle ridges have been superposed by crater ejecta, and the ejecta is embayed by some modest postimpact volcanism.

[49] The overall sequence of events observable in the vicinity of Greenaway begins with formation of heavily deformed tessera terrain. Formation of regional volcanic plains covered much of the area so that only high-standing remnants of the tessera remain exposed. Modest deformation of the plains then occurred with the formation of wrinkle ridges. Crater formation postdates wrinkle ridge formation and occurred in the presence of a slight NW-SE regional topographic slope. There was some modest postimpact volcanism, perhaps tens of meters from numerous edifices, that embayed portions of the ejecta blanket primarily north and west of the crater.

4.5. Potanina, Latitude 31.7°N, Longitude 53.0°E, Diameter 90 km

[50] Potanina is located on the northeastern edge of flows associated with Nyx Mons, one of the large shield volcanoes

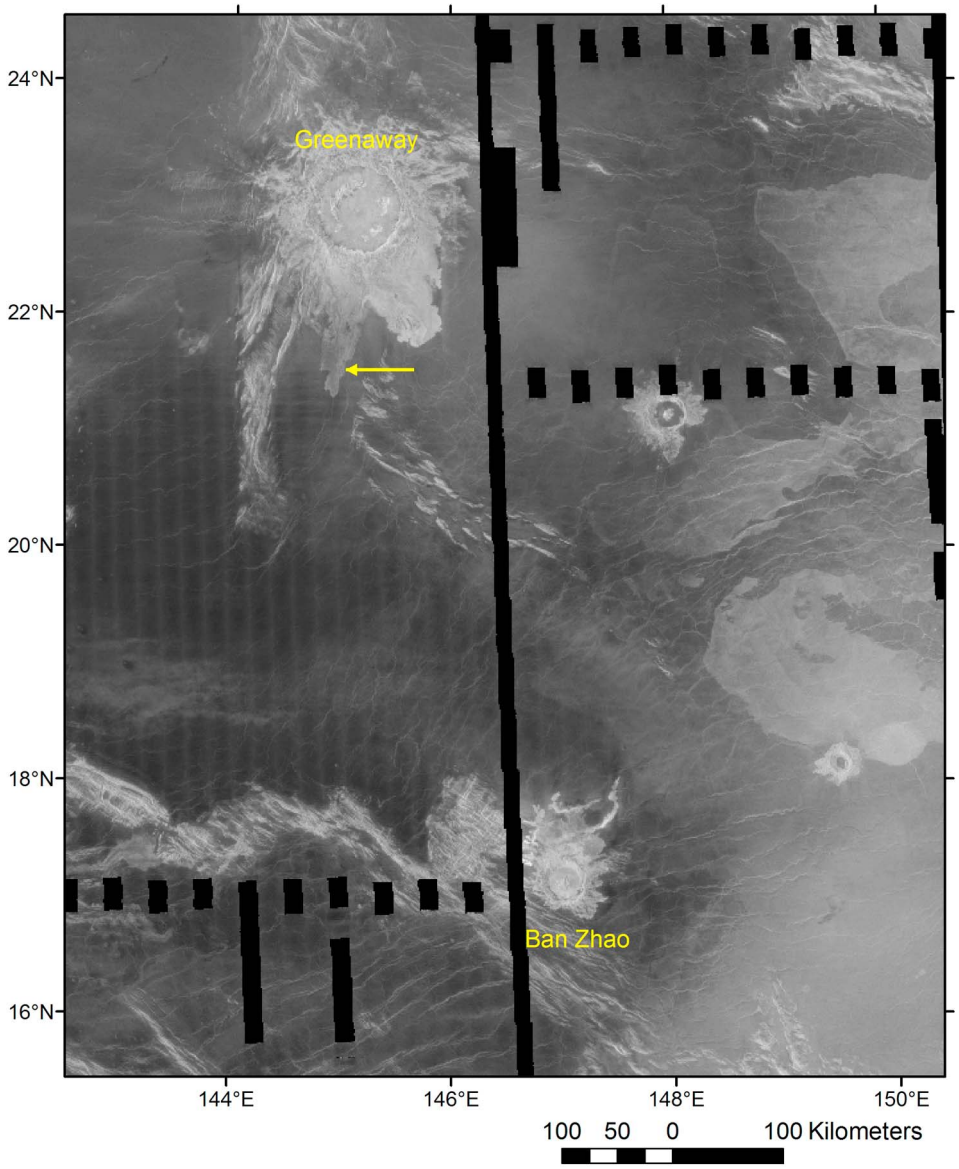

Figure 20. Regional image showing Greenaway crater (22.9°N, 145.1°E, D = 92 km) and surroundings. Arrow indicates flow of Greenaway ejecta that may have been darkened by materials from the extended parabola associated with Ban Zhao crater.

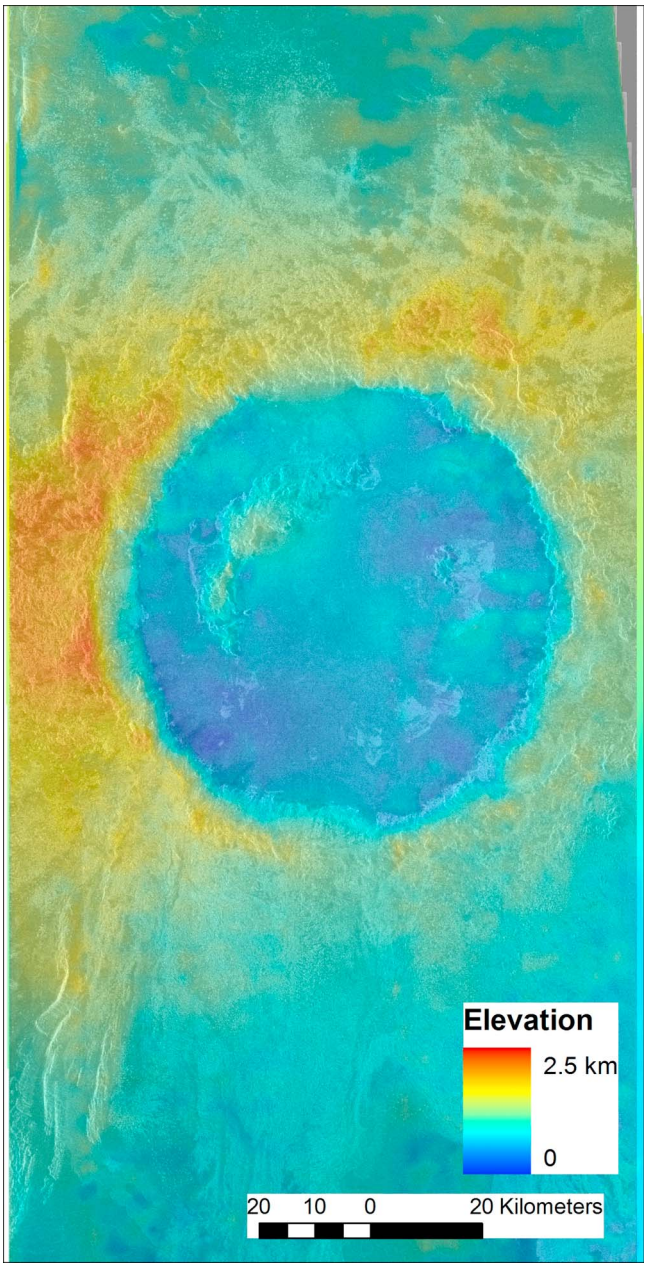

Figure 21. Topography of Greenaway superposed on cycle 1 imagery. Note that the northwest rim and peak ring are higher than in the southeast, but the crater floor is flat. Also, north of the crater only high-standing areas have ejecta on them. There is a data gap in the cycle 3 imagery in a 20 km N-S strip through the middle of the crater, and topography has been interpolated across the gap.

in Bell Regio (Figure 23). The summit of Nyx Mons is ~300 km east of Tepev Mons, and the gravity signals associated with these two edifices have some overlap at longer wavelengths [*Herrick et al.*, 2005]. There are flows from Tepev that clearly postdate flows associated with Nyx, but the substantial free air anomalies of both features and their relationships to surrounding terrain indicates that both volcanoes are relatively recent features that may still be active [*Herrick et al.*, 2005]. Remnants of tessera terrain outcrop ~100 km southeast of the rim and appear to divert some of the flows associated with the crater's ejecta.

[51] The rim of Potanina has a constant elevation on its perimeter, and the floor of Potanina exhibits no clear regional tilt. The crater interior has no fully contiguous rings, but the exposed arcs appear more consistent with two, rather than one, interior rings. The area inside these partial rings is 100–150 m lower in elevation than the rest of the crater floor and has a set of polygonal lineaments (Figure 24). The interior of the crater contains a plateau on its east side that sits ~400 m higher than the remainder of the area outside the rings. Only the east side of the crater has a rim that is significantly elevated above the surrounding terrain. The ejecta also appears more continuous and brighter in this area. Portions of the floor on the eastern side of the crater interior are radar bright and appear to be embayed by darker material that covers the floor and embays the peak rings. The west side of the crater floor has a lower backscatter than radar-dark areas exterior to the crater.

[52] We infer from our mapping that formation of the tessera that is southeast of the crater was one of the earlier events in the region. Emplacement and modest wrinkle ridge deformation of volcanic plains that embay the tessera also occurred prior to Potanina's formation. The plains generally have no obvious source region. Potanina then formed before the last visible flows from Nyx. The ejecta from Potanina flowed to the east, was diverted by the tessera, and clearly flowed over some of the wrinkle ridges. Some of the flows

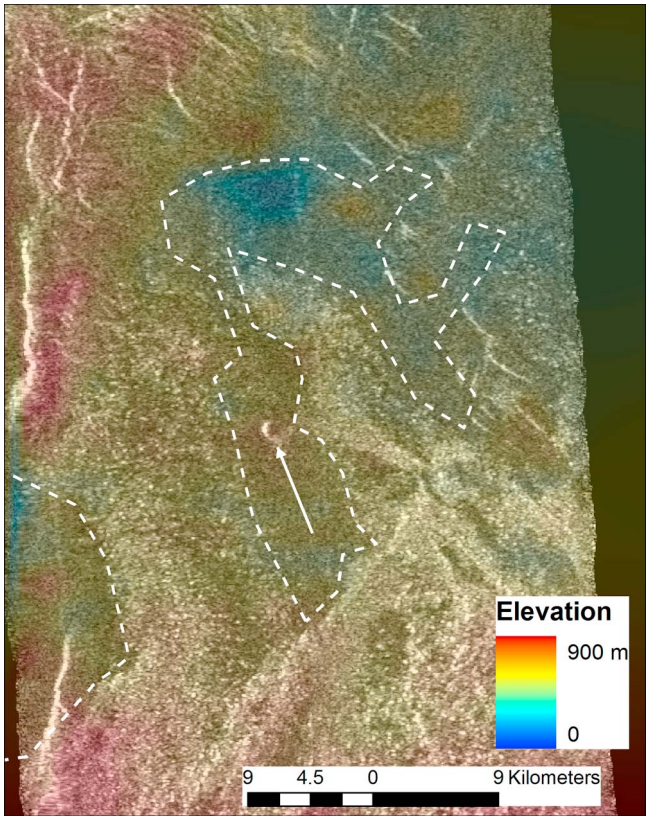

Figure 22. Close-up view of northwest portion of ejecta for Greenaway showing approximate boundaries of later lavas that flowed into low-lying areas and superposed the ejecta blanket. Arrow indicates possible small volcano.

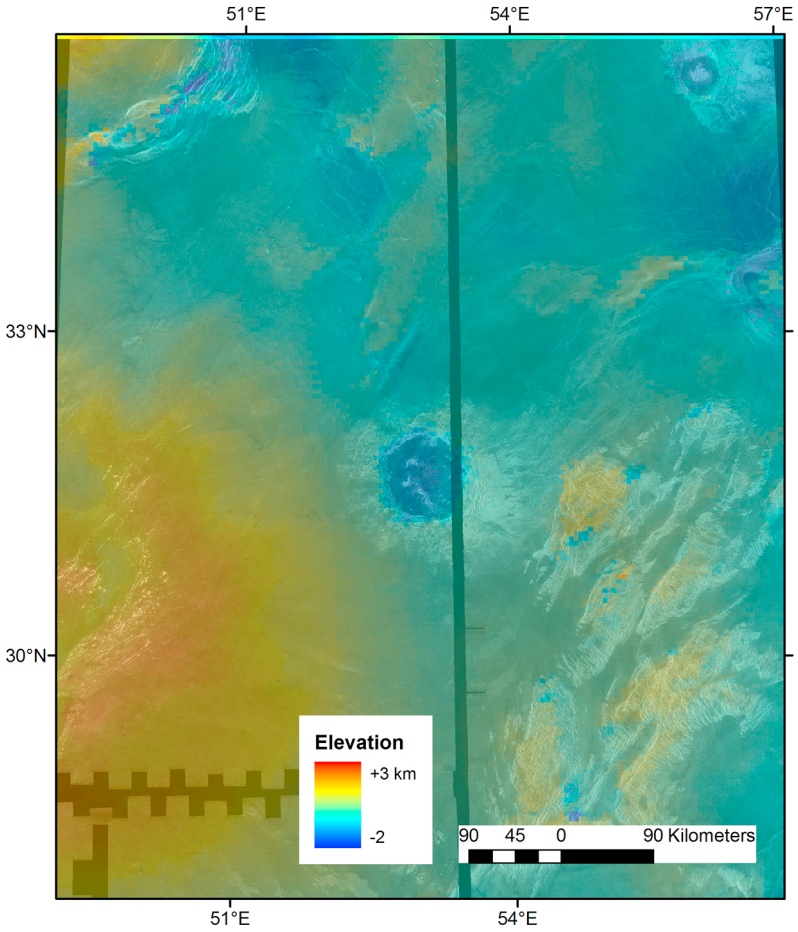

Figure 23. Regional (GTDR) topography of Potanina (31.7°N, 53.0°E, D = 90 km) superposed on cycle 1 imagery. Nyx volcano is the elevated feature to the southwest, and ejecta flows to the east associated with the crater follow the regional topographic trend. Elevations are relative to mean planetary radius of 6051.8 km.

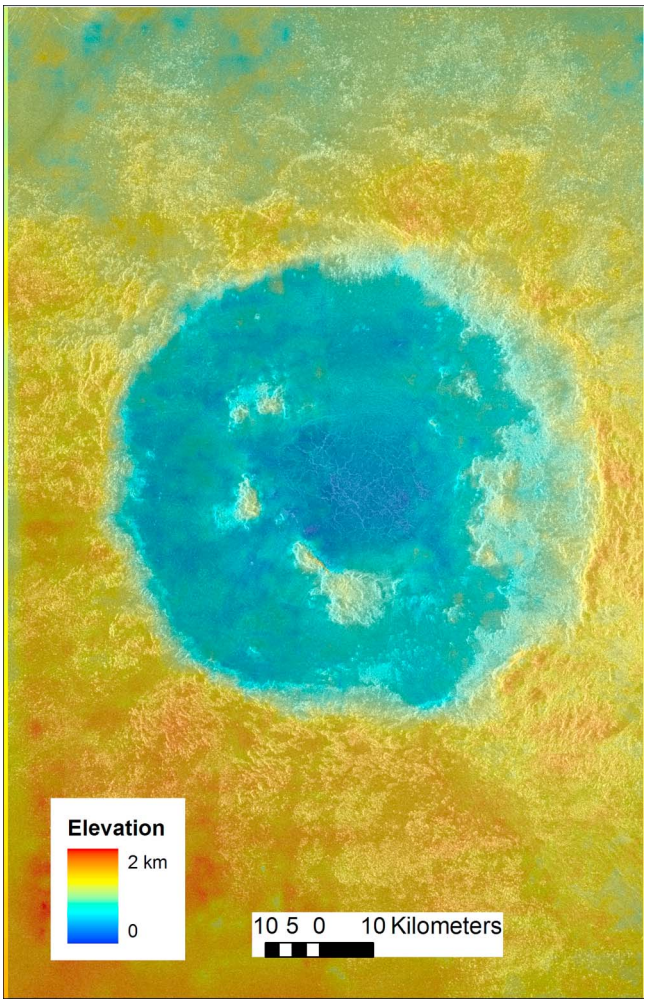

Figure 24. Stereo-derived topography (relative elevations) superposed on imagery for interior and rim of Potanina. Only the eastern rim is elevated above the surrounding terrain. The area inside the peak ring is lower than the remainder of the crater interior and has polygonal lineaments.

originate in dark areas in the ejecta blanket and have no apparent source. These may be flows that originate from the ejecta blanket after its main deposition has stopped. After formation of Potanina, flows from Nyx Mons covered much of the ejecta and may have spilled into the crater interior (Figure 23). Combined thicknesses of crater-embaying flows were probably a few hundred meters. The preservation of substantial topography within the crater interior, namely the distinctly lower region inside of the peak ring, suggests that flooding of the crater interior by Nyx flows was minimal.

4.6. Markham, Latitude 4.1°S, Longitude 155.6°E, Diameter 72 km

[53] The regional setting for Markham is in Rusalka Planitia approximately 200 km north of Nuahine Tessera (Figure 25). Adjacent to Markham to the west is an unnamed corona centered at 4.0 S, 154.8 E with a diameter of 150 km. That corona is just southeast of the multiringed Seia Corona, located at 30.0 S, 153.0 E with a diameter of 225 km. Ejecta is not present exterior to the west and southwest rim, and the rim there is lower than for the remainder of the crater. The rim is otherwise at a constant elevation, and the floor is flat, so we conclude that no significant postimpact tectonic tilting has occurred. There is a topographic trough extending from the crater rim to the northeast that may reflect ricocheted projectile material gouging out a portion of the rim. The trough, the southwest "forbidden zone," and the overall ejecta pattern lead us to interpret the crater to have formed from an oblique impact coming from the southwest.

[54] Radar-bright ejecta flows extend to the east a few hundred km away from the crater. These flows follow the regional topography downslope to the east. Generally wrinkle ridges in the plains are crosscut, and therefore superposed, by the Markham flows. However, in a few places the wrinkle ridges can be traced within the flows. Either those wrinkle ridges formed or were reactivated after Markham's formation, or the Markham flows overran the wrinkle ridges but later settled to reveal their underlying topography. At their termini the flows pond against and are diverted by the wrinkle ridges in the plains. We interpret most of the wrinkle ridges to have been existing structures at the time of impact, but cannot rule out that some of them may postdate Markham.

[55] The relationship between Markham and the unnamed corona immediately to the west is not entirely clear. There is no evidence that the topography of the corona has directly affected the flow of the ejecta from the crater. If the current corona topography existed at the time of impact, then we might expect the ejecta to have flowed into the corona's central low. To the west-northwest of the crater it appears that an area associated with the corona, the ejecta, and into the floor of Markham was embayed by volcanic flows (Figure 26). That there is now a topographic arch through the middle of these embaying flows suggests that formation of the topographic structure of the corona postdates the crater and the embaying and filling flows. In other words, we interpret that the corona was more domical when the flows were emplaced, and the central corona low formed later as the corona completed its collapse [e.g., *Janes et al.*, 1992].

[56] As was noted by *Herrick and Sharpton* [2000], the craters like Markham with extensive outflows seem to be located in close proximity to significant volcanic structures (in this case a corona). We did not identify any evidence of postimpact volcanism associated with the Markham ejecta outflows. *Schultz* [1992] suggested that landing on an active corona structure may have meant that substantially more melt and vapor was incorporated into the ejecta and resulted in the enhanced outflows. This interpretation is consistent with our observations.

[57] Our overall interpretation of the regional sequence of events is consistent with the mapping of *Hansen and DeShon* [2003]. Nuahine Tessera outcropping south of Markham was the first unit to form. Flows associated with Seia and the unnamed corona adjacent to Markham formed regional lava plains that embayed the tessera. Fracturing associated with corona formation and most of the wrinkle ridge deformation of the plains predates Markham. Some modest wrinkle ridge deformation may postdate Markham, but the evidence for this is not conclusive. Volcanism associated with the immediately adjacent corona embayed the western ejecta blanket and flowed into the crater interior (combined thicknesses of flows of a few hundred meters). The adjacent corona continued to evolve and subsequently developed its central low.

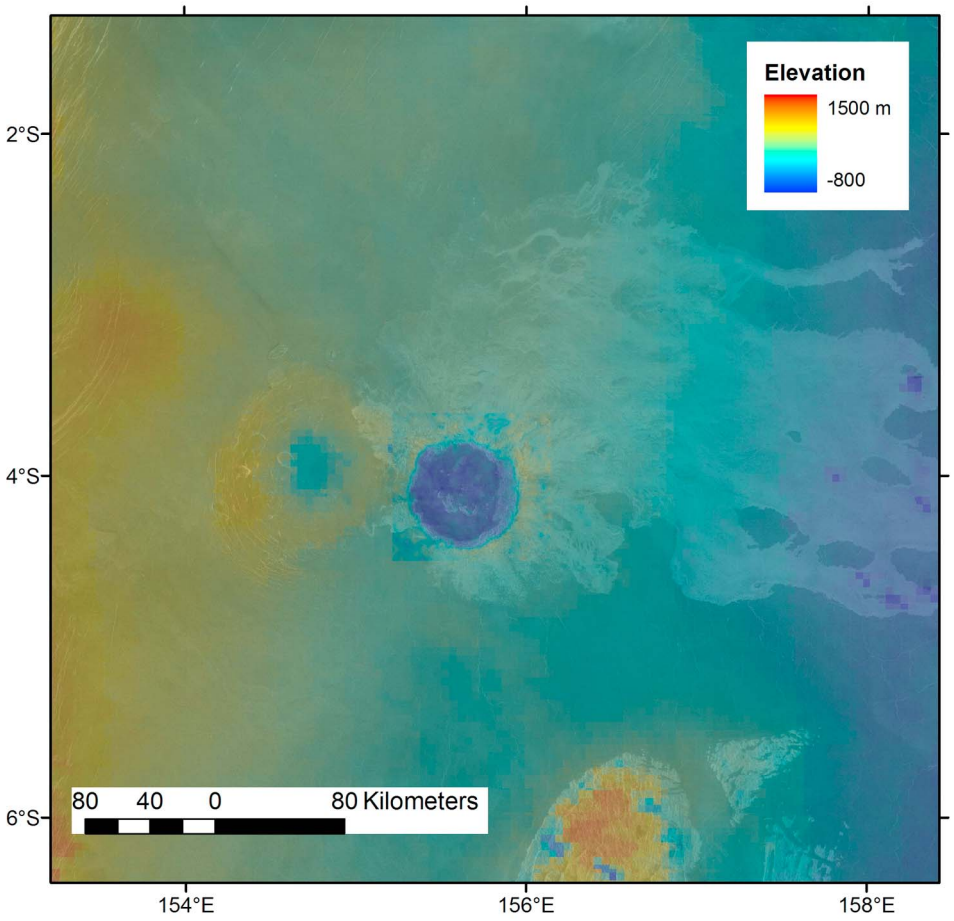

Figure 25. Regional view showing Markham (4.1°S, 155.6°E, D = 72 km) on flank of unnamed corona to the west. Remnants of Nuahine Tessera are on the southern edge of the image. Note that the flows from Markham follow the regional topography and that there is no topographic expression of the rim on the west and southwest.

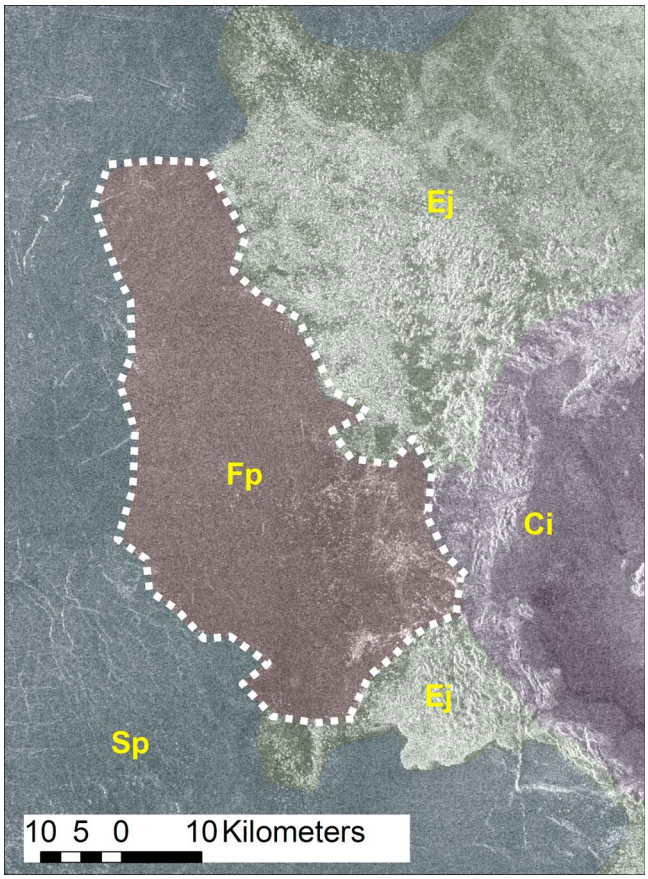

Figure 26. Dashed line shows approximate boundary of smooth flows (featureless plains unit Fp) that embay both ejecta (EJ unit) and corona-related structures (in smooth plains unit Sp) and that may have flowed into Markham (crater interior unit Ci).

4.7. Hepworth, Latitude 5.1°N, Longitude 94.6°E, Diameter 63 km

[58] Hepworth and de Beauvoir (discussed below) are located ~350 km apart on the northeastern edge of Ovda Regio, a large tessera area in Aphrodite Terra (Figure 27). Hepworth straddles the boundary between a tessera block and an embaying unit of volcanic plains to the south. North of the crater rim, in the tessera block, there are a few patches of ejecta visible on areas of high-standing tessera, but most of the area north of the crater shows little ejecta. There is abundant evidence that the northern rim has been deformed by processes associated with the tessera deformation (Figure 28); this is similar to the deformation of the eastern rim of Joliot-Curie. The remnants of the northern part of the peak ring are elevated several hundred meters relative to the remainder of the peak ring, and this indicates that the faulting of the northern portion of the crater involves substantial vertical displacement. It is also clear that volcanic flooding of the crater interior has occurred. In contrast, the south and southeastern portion of the rim shows no evidence of deformation. In these areas the ejecta is well preserved and was emplaced on flat volcanic plains.

[59] The postimpact tectonic and volcanic activity is not limited to the northern portion of the crater. The abrupt termination of the ejecta blanket to the south at the point of a step down in topography suggests that there was vertical displacement along an east-west striking fault, and the lower southern block was subsequently covered by volcanic flows (Figure 28). One can also trace a north-south striking fault through the crater interior and into the tessera north of the crater (Figure 28). This fault within the flooded crater floor clearly indicates that postimpact activity included multiple deformation episodes interspersed with volcanism.

[60] With respect to the regional sequence of volcanic and tectonic events, it is clear that a substantive amount of activity postdates formation of Hepworth. It is unknown exactly how flat the terrain was that the crater was deposited on. However, the lack of much remaining ejecta and the extensive deformation for the northern portion of the crater indicates that much of the tessera deformation postdates the crater. The preservation of ejecta to the south of the crater rim indicates that part of the crater was emplaced on volcanic plains that predate the crater. However, some volcanism clearly occurred interspersed with the tectonic activity that postdates the crater. Overall, some of the faulting appears to have involved hundreds of meters of vertical throw, and perhaps a few kilometers of horizontal movement, and the level of volcanic burial requires cumulative flow thicknesses of hundreds of meters.

4.8. Carreno, Latitude 3.9°S, Longitude 16.1°E, Diameter 57 km

[61] Carreno is located in the plains of Tinatin Planitia, a few hundred kilometers northeast of a partially buried chain of coronae that includes Heng-o Chasma (Figure 29). The area has pervasive west-southwest striking wrinkle ridges that are orthogonal to parallel fractures and graben. The orthogonality suggests that the wrinkle ridges and graben could be contemporaneous features that formed under the same stress field. In several areas it appears that graben affected wrinkle ridge formation by truncating the wrinkle ridges or altering their strike, so certainly the graben do not postdate the wrinkle ridges (Figure 30a). Both the wrinkle ridges and graben are, generally, covered by the crater's near-rim ejecta (Figure 30a). No wrinkle ridges or graben deform the crater rim or floor. We conclude that the bulk of wrinkle ridge and graben deformation precedes crater formation. However, in one place the graben can be traced through the ejecta blanket, so at least some graben activity postdates the crater (Figure 30b).

[62] There is also some evidence for modest postimpact volcanic activity in portions of the region. The floor of Carreno is radar-dark with a backscatter similar to the surrounding plains. To the southeast of the crater it appears that the wrinkle ridges controlled the flow of ejecta material, and there appear to be the remnants of a dark halo northeast of the crater. However, in areas north and west of the rim the bright, blocky ejecta appears on the crest of the wrinkle ridges, and the low-lying areas are radar dark. In these places it may be that flows from small, unimaged volcanoes covered the radar-bright ejecta (Figure 30a). There also appears to be the remnants of a companion crater to the west, but there is no way to evaluate whether that feature formed contemporaneously with Carreno. That feature clearly postdates the regional wrinkle ridges, and if it is an impact structure then it has clearly been filled by postimpact lavas.

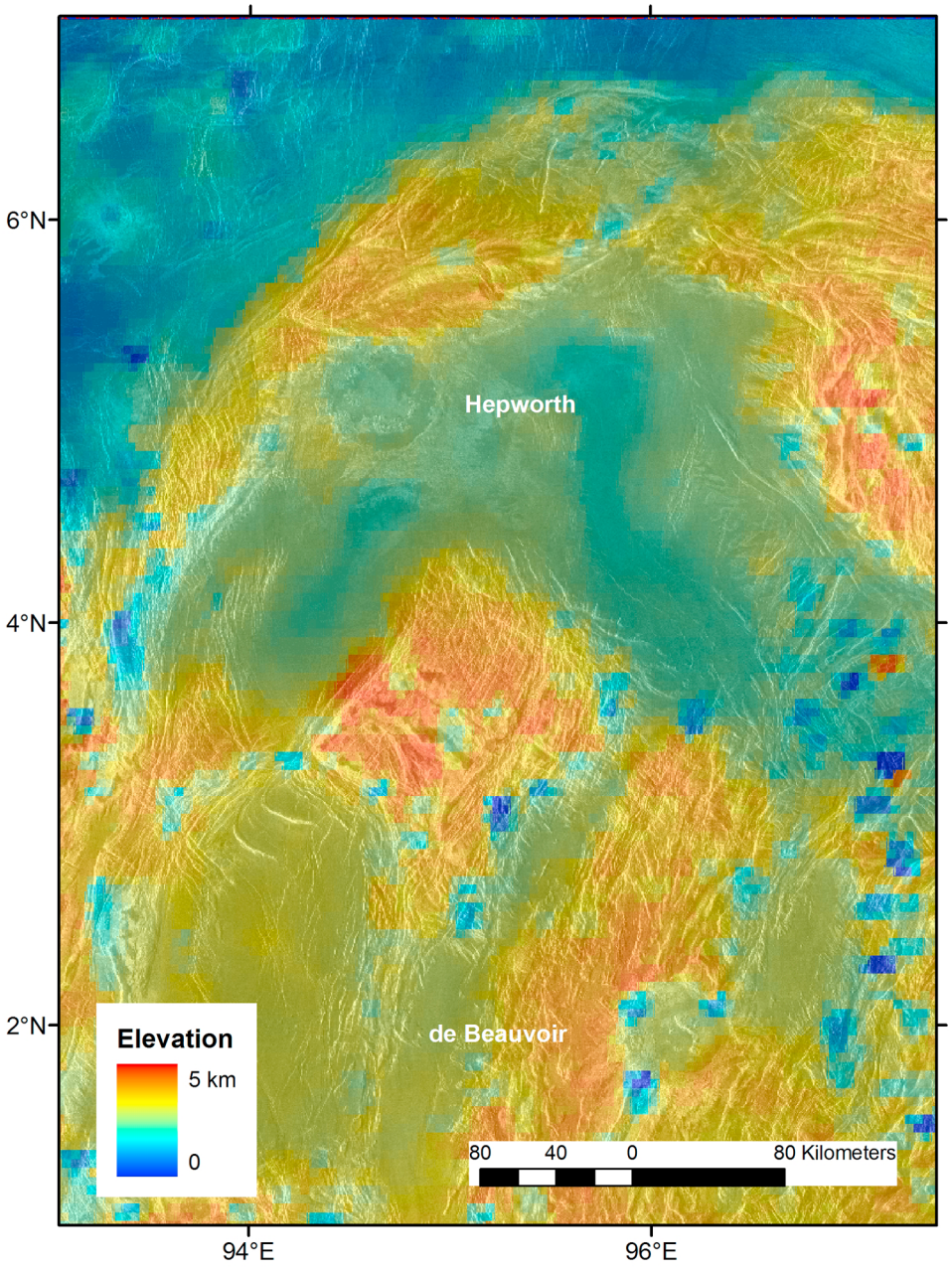

Figure 27. Regional view showing Hepworth (5.1°N, 94.6°E, D = 63 km) and de Beauvoir (2.0°N, 96.1°E, D = 53 km) in Ovda Regio. Hepworth straddles a tessera-plains boundary near the northern boundary of Ovda, and de Beauvoir is located on some of Ovda's highest tessera terrain.

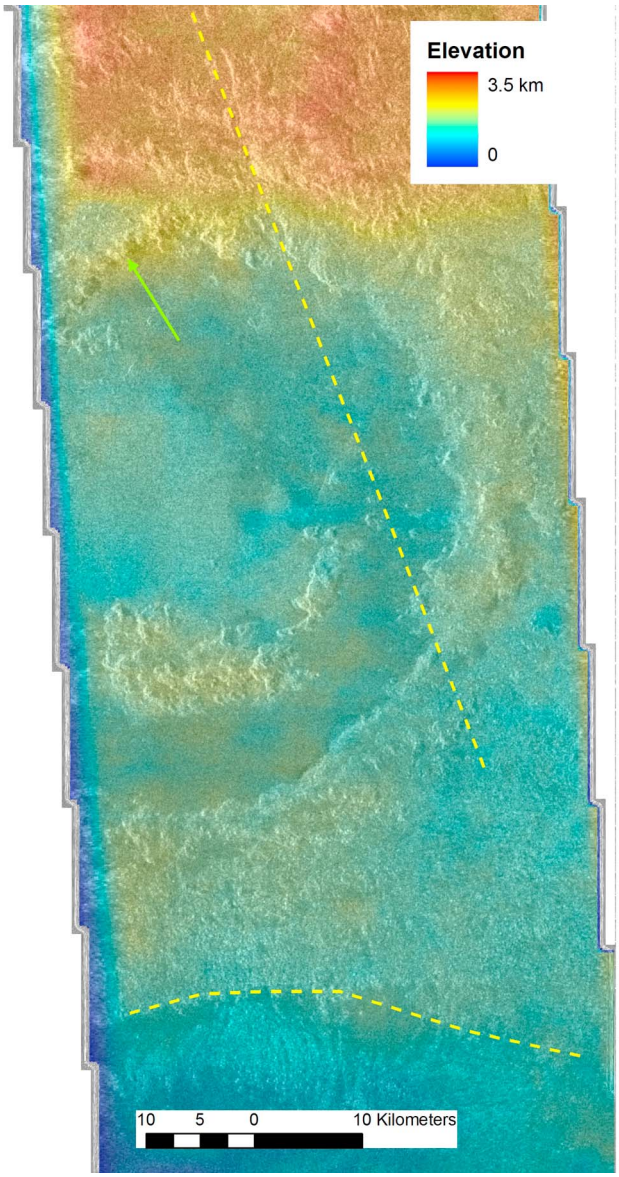

Figure 28. Detailed view of Hepworth. Note preservation of ejecta south of the crater but lack of ejecta in intratessera troughs north of the crater. Green arrow points to elevated remnants of peak ring. North-south trending straight line indicates strike of fault that cuts through a subsequently flooded crater floor. East-west trending dotted line indicates topographic step, south of which the ejecta is partially embayed by later radar-dark flows.

[63] Our interpretation of the regional geologic history indicates that only modest postimpact activity occurred. The regional lava plains were the first features to form in the region. The regional deformation that produced the orthogonal pattern of graben and wrinkle ridges then occurred. Formation of Carreno and the small crater to the west postdates this deformation. There may have been some later modest (tens of meters or less cumulative thickness) volcanic flooding of the companion crater, portions of the ejecta blanket, and the crater floor. Some minor reactivation of existing grabens and wrinkle ridges may also have occurred.

4.9. De Beauvoir, Latitude 2.0°N, Longitude 96.1°E, Diameter 53 km

[64] As mentioned above, de Beauvoir is in Ovda Regio about 350 km south-southeast of Hepworth (Figure 27). While Hepworth straddles a plains-tessera contact near the northern edge of Ovda, de Beauvoir sits on top of some of the region's highest tessera terrain. The ejecta is best preserved adjacent to the west and south of the rim (Figure 31). Here the ejecta appears to cover both high-standing and low-standing tessera areas; these areas are also relative highs. The ejecta east and northeast of the rim is only preserved on a few high-standing remnants of tessera. In these areas, the valleys that are between high-standing tessera blocks appear to be flooded by smooth plains material that we interpret to be volcanic in origin. There also appears to be connected flooding from the intertessera blocks to the crater interior.

[65] There is evidence that some of the deformation in the tessera postdates formation of the crater. The peak ring of de Beauvoir is asymmetric, and we interpret the crater floor and peak ring to have been deformed and subsequently embayed in a manner analogous to Joliot-Curie. We interpret the deformation of the peak ring to be associated with a regional thrust fault that strikes north-northwest (Figure 31). There also appears to be some deformation of the eastern rim of crater (Figure 31).

[66] There is considerable variation in the rim-floor elevation. The western and northwestern portions of the rim are as much as 1500 m above the floor. To the east the tessera blocks in the rim are only ~800 m above the floor. The lowest intertessera troughs, which have no ejecta and appear to

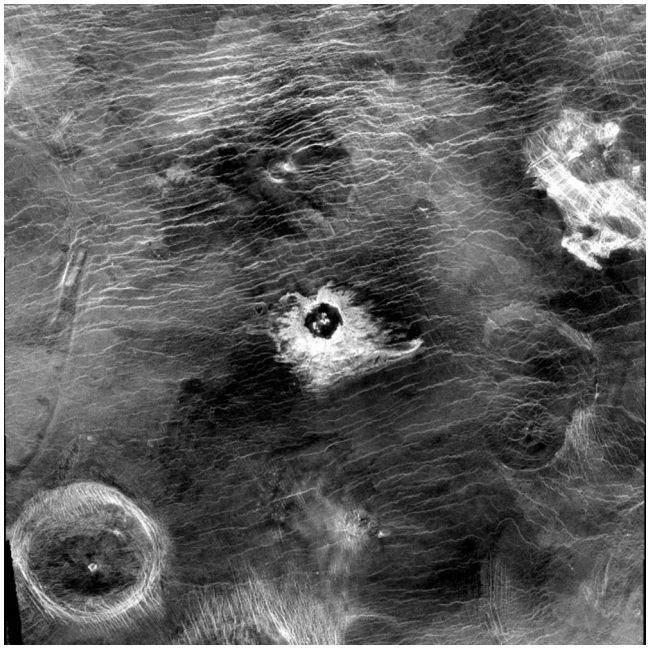

Figure 29. Regional image 850 × 850 km (0 to 7.9°S, 12.2 to 20.1°E) showing Carreno (3.9°S, 16.1°E, D = 57 km). Note corona structures to the southwest and other volcanic structures south and north. Area is pervaded by west-southwest striking wrinkle ridges and an orthogonal set of straight fractures and graben. There is also the rim outline of what may be a companion crater ~50 km west-northwest of the crater.

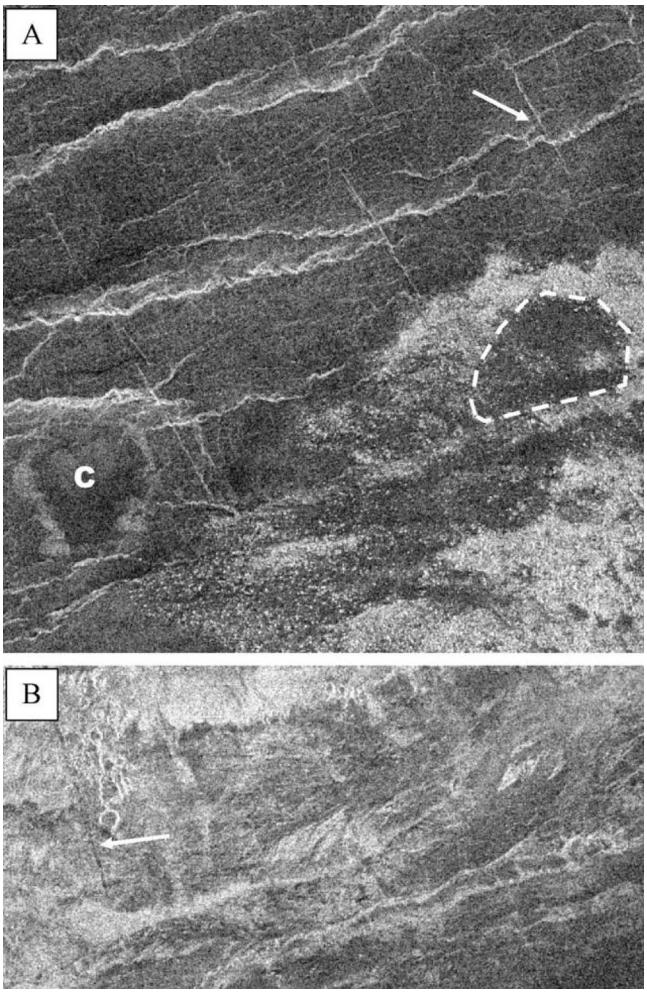

Figure 30. Close-up images of Carreno. Both images are 60 km across. (a) Area northwest of the crater shows graben structures that alter wrinkle ridge formation (e.g., arrow), ejecta that clearly superposes wrinkle ridges, potential embayment of ejecta by radar-dark flows (e.g., area enclosed by dashed line), and potential companion crater ("C"). (b) Area south of crater that appears to show graben cross-cutting ejecta (best example at arrow).

connect flooding from crater exterior to crater floor, are only 300–400 m higher than floor elevation.

[67] The overall history for de Beauvoir has some similarity to Joliot-Curie. Most of the tectonic and volcanic activity in Ovda Regio predates de Beauvoir. There was significant tectonic folding involved in forming the tessera, and troughs in the tessera are embayed by volcanic flows. The large rim-floor depth on the west side of the crater, the preserved circularity of the rim, and the preservation of ejecta to the west and northwest, including in the troughs, suggests that little postimpact activity has occurred on that side of the crater. In the eastern half of the crater at least some deformation postdates the crater, particularly deformation of the peak ring associated with a north-northwest striking fault. Post-deformation volcanic flows have covered faults in the crater floor and low-standing ejecta to the east and southeast. In the eastern portion of the crater cumulative thickness of volcanic flows must be at least a few hundred meters, and postimpact strain levels associated with faulting are less than a few percent.

4.10. Langtry, Latitude 17.0°S, Longitude 155.0°E, Diameter 52 km

[68] Langtry is located on the edge of Diana Chasma in a portion of the chasma just southeast of the 700 km diameter Ceres Corona (Figure 32). The crater is heavily deformed by east striking extensional structures and northwest striking extensional structures (Figure 33). These fractures, faults, and graben are associated with formation of the chasma and coronae. None of this deformation is truncated by the impact structure in the imagery, and the topography also shows that the fault throws are continuous through the crater. We interpret all of the deformation associated with chasma and corona formation in the immediate area as postdating the crater.

[69] Around two-thirds of the periphery of the crater are preserved remnants of an ejecta blanket, and there are some radar-bright patches that may be ejecta between the rim and peak ring. The ejecta is poorly preserved east of the crater, and this area is topographically low. Within the peak ring is an area that is more radar dark than the remainder of the crater interior. Throws on some of the faults are a few hundred meters. The rim-floor height is low for a crater of this size and is only a few hundred meters. The crater is too heavily deformed to allow reliable estimation of the rim height.

[70] Our interpretation is that Langtry predates the local formation of Diana Chasma. Between crater formation and the pervasive faulting, some volcanism (as much as a few hundred meters cumulative thickness) partially filled the crater interior and embayed portions of the ejecta.

4.11. Warren, Latitude 11.7°S, Longitude 176.5°E, Diameter 49 km

[71] Warren is located in the middle of Dali Chasma just south of Sith Corona. Sith is one of several coronae connected by the Dali Chasma rift system, and Warren is located within the portion of the rift that makes up the southern annular trough of Sith. Warren has a very unusual appearance, and even with stereo-derived topography its history is difficult to interpret (Figure 34). Despite obvious deformation, the structure maintains circularity and the floor is flat. There is some ejecta preserved on the rim to the east and northeast, and there are preserved patches of ejecta in the crater's surroundings, predominately in high-standing areas. Only the northern half of the crater floor has a central structure; it is a crude semicircle of mountains. Topography shows a crater wall of at least a few hundred meters completely surrounding the floor, but to the northwest the wall does not have the typical terraced wall of a complex crater.

[72] Regional mapping by *Hansen and DeShon* [2003] interprets Warren as being flooded by both radar-bright and radar-dark flows, an interpretation with which we concur. North of the crater rim there are ejecta-free radar-dark patches in low-standing areas. There are clear conduits from some of these patches down to the radar-dark portion of the crater floor. There are isolated radar-dark patches within the radar-bright material in the southern part of the floor. Either these are kipukas of the dark-floored material, or there are isolated volcanic features without visible source vents contained within the bright material. The lack of discernible features or higher elevations within the isolated patches leads us to

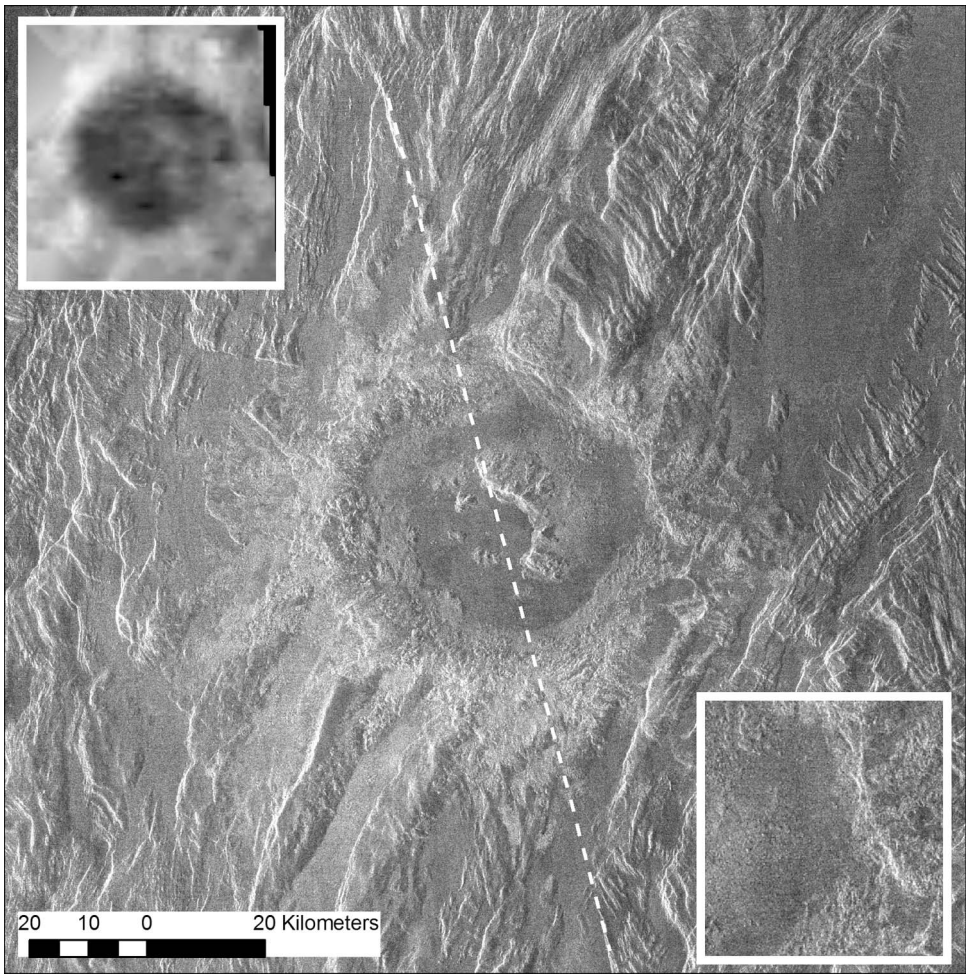

Figure 31. The de Beauvoir impact structure. Dashed line shows approximate strike of inferred fault that produced asymmetric central structure. Top, left inset shows stereo-derived topography (1500 m total relief in area shown). Bottom, right inset highlights evidence of postemplacement deformation of crater rim.

interpret the radar-bright material as later flows superposed on radar-dark flows that had previously flooded portions of the crater interior. There is radar-bright material southwest of the crater rim that has the same elevation and backscatter as the radar-bright portion of the crater interior, and we interpret these areas as having experienced flooding by radar-bright flows.

[73] The topography of the crater and surroundings is particularly valuable in inferring preimpact and postimpact deformation. In the southern half of the crater, the rim-floor height ranges from 300 to700 m. In the northern part of the crater, the rim ranges from 1 to 1.8 km in elevation above the floor, and the highest part occurs where there is no obvious preserved ejecta. Typical fresh craters in this size range have a rim-floor depth of 1 km. The remnants of the central structure look deformed and stand 300–400 m above the floor. The topography shows a west-northwest striking scarp that parallels the southern boundary of the central structure. We interpret this as a postimpact fault, and the southern block must have dropped at least 400 m in order for the southern portion of the central structure to be covered by later infilling of the crater. Finally, there is a north-northwest trending feature that we interpret as a thrust fault that runs through the rim and the preserved part of the central peak, and the upthrown block is to the east.

[74] Warren and its immediate surroundings have clearly experienced a complicated history. The exceptionally high rim-floor elevations in the northern portion of the crater suggest to us that significant deformation predated crater formation, and the impact occurred into very rugged terrain. After the impact, thrust faulting striking north-northwest elevated the eastern portion of the crater and deformed the central structure. Subsequent radar-dark volcanic flooding partially covered but did not remove the northwest rim, partially filled the crater interior, and embayed much of the crater exterior. The southern portion of the crater was then downdropped somewhere between 500 m and 1 km along a west-northwest striking fault. Finally, radar-bright flows embayed and filled the crater in its southern and western portions.

4.12. Voynich, Latitude 35.3°N, Longitude 56.1°E, Diameter 48 km

[75] Voynich is located in volcanic plains in Bell Regio ~500 km northeast of Potanina and ~700 km east of Nefertiti Corona. The local topography is flat and the plains upon which Voynich sits cannot be clearly identified as flows from

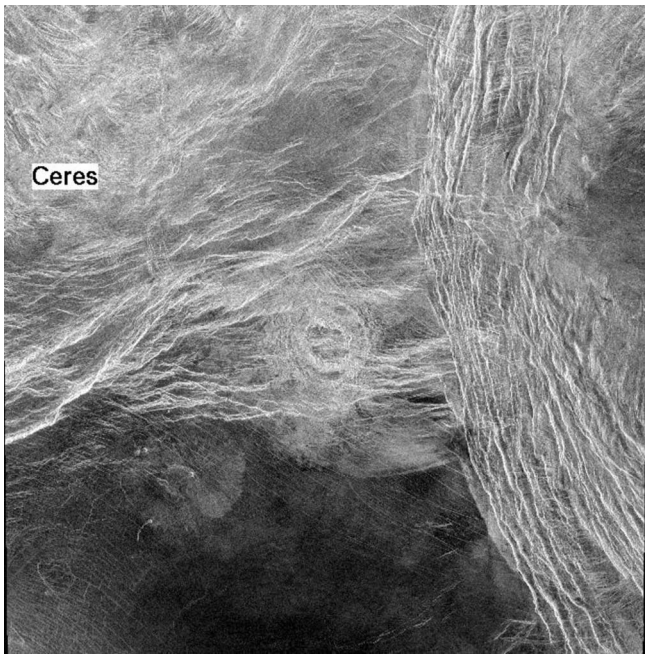

Figure 32. Regional view 400 × 400 km (15 to 18.8°S, 153 to 157.1°E) showing Langtry (17.0°S, 155.0°E, D = 52 km) located in the Dali-Diana Chasma structure southeast of Ceres corona.

one of the nearby major volcanic edifices despite its proximity to them (Figure 35). Initial regional mapping by *Campbell and Rogers* [1994] shows Voynich at the top of the stratigraphic column and superposed on two regional plains units, and the later map by *Campbell and Campbell* [2002] also superposes the crater on regional plains.

[76] The plains surrounding Voynich have orthogonal patterns of wrinkle ridges that do not deform the crater floor or rim. Near the crater rim the wrinkle ridges appear to be superposed by the ejecta. Farther from the rim, however, it appears that the wrinkle ridges diverted ejecta flows and altered the depositional albedo pattern (Figure 36a). These observations lead us to interpret Voynich as postdating the regional wrinkle ridge deformation.

[77] The backscatter of the floor of Voynich is similar to the surrounding plains except for the radar-bright floor within the crater's small peak ring. Unfortunately there is a data gap in the stereo coverage through the middle of the crater, so we cannot determine if the radar-bright floor area is high-standing. The rim-floor depth is only ~200 m below the trend for bright-floored craters. We interpret that there is minimal, if any, postimpact filling of the interior. However, in the north and east portions of the ejecta blanket there are clearly high-standing small volcanic edifices. There are radar-dark flows associated with some of these edifices that superpose and crosscut ejecta flows from Voynich (Figure 36c).

[78] In the area surrounding Voynich we interpret the first event to be deposition of regional volcanic plains. Wrinkle ridge deformation of these plains preceded formation of Voynich. After formation of Voynich, radar-dark flows, probably no more than tens of meters thick, from small volcanic edifices covered portions of the ejecta blanket, and there may have been some volcanic flooding of the crater interior.

4.13. Summary of Geologic Histories of Large Craters

[79] The large craters that we studied show a spectrum of postimpact volcanism and deformation (Table 4), and only Cleopatra could be interpreted as completely unmodified. A few have volcanic flows with thicknesses of less than tens of meters covering minor portions of the interior and ejecta, while others have experienced multiple episodes of significant faulting interspersed with volcanic filling and/or embayment. Some of the craters have throughgoing faults with hundreds of meters of throw, and volcanism has nearly filled some craters and surrounded them to nearly the elevation of the rim. None of these structures, however, have experienced significant amounts of horizontal strain, and they are all still circular.

[80] As a brief aside, we compare our results with those of *Brown and Grimm* [1996], who used altimetry with imagery to examine twelve large craters on Venus to look for viscous relaxation and thermal subsidence effects. Stereo-derived topography for Mead [*Herrick and Sharpton*, 1996], Cleopatra, Maria Celeste, and Potanina are consistent with their interpretation that postimpact thermal subsidence occurs in the central areas of large craters. With limited examples, our more detailed topography suggests that the subsidence is restricted to within the peak ring. We did not have adequate stereo coverage through the crater center to allow assessment of thermal subsidence for Joliot-Curie or Greenaway, two other craters in our detailed studies that overlapped with those studied by *Brown and Grimm* [1996]. While *Herrick and Sharpton* [1996] interpreted that the stereo-derived topography showed viscous relaxation for Mead that *Brown and Grimm* [1996] did not see in the altimetry data, our results for all of the craters examined here concur with the interpretation by *Brown and Grimm* [1996] that viscous relaxation does not generally occur for Venusian craters.

5. Discussion and Conclusions

[81] An extensive body of past work has shown that when a Venusian impact crater forms, it will have a low-backscatter halo beyond the continuous radar-bright ejecta blanket, and the interior floor will have high backscatter (be radar bright) relative to the surrounding terrain. Sedimentary processes or surface weathering may cause the floors of a few craters to develop over time backscatter properties similar to the surrounding terrain. The depth and rim height data presented here and in previous works argues, however, that a radar-dark floor in a crater is most likely an indicator that a crater has been embayed and partially filled by volcanic flows. Dark-floored craters make up ~80% of the crater population above ~16 km in diameter, with this percentage not significantly varying with increasing size [*Herrick and Phillips*, 1994]. Smaller craters usually have bright, but not topographically flat, floors. Our observations of dark halos, our mapping of large craters, and photogeologic observations of others [e.g., *Izenberg et al.*, 1994], indicate that the embayment and infilling often occurs with events that are of limited areal extent, so sometimes portions of an impact structure remain pristine while other portions are being resurfaced. Cumulative thicknesses of hundreds of meters of lava flows filling and embaying a crater are common. Observed strain levels were always less than a few percent, but it is common for episodes of faulting to be interspersed with postimpact volcanism.

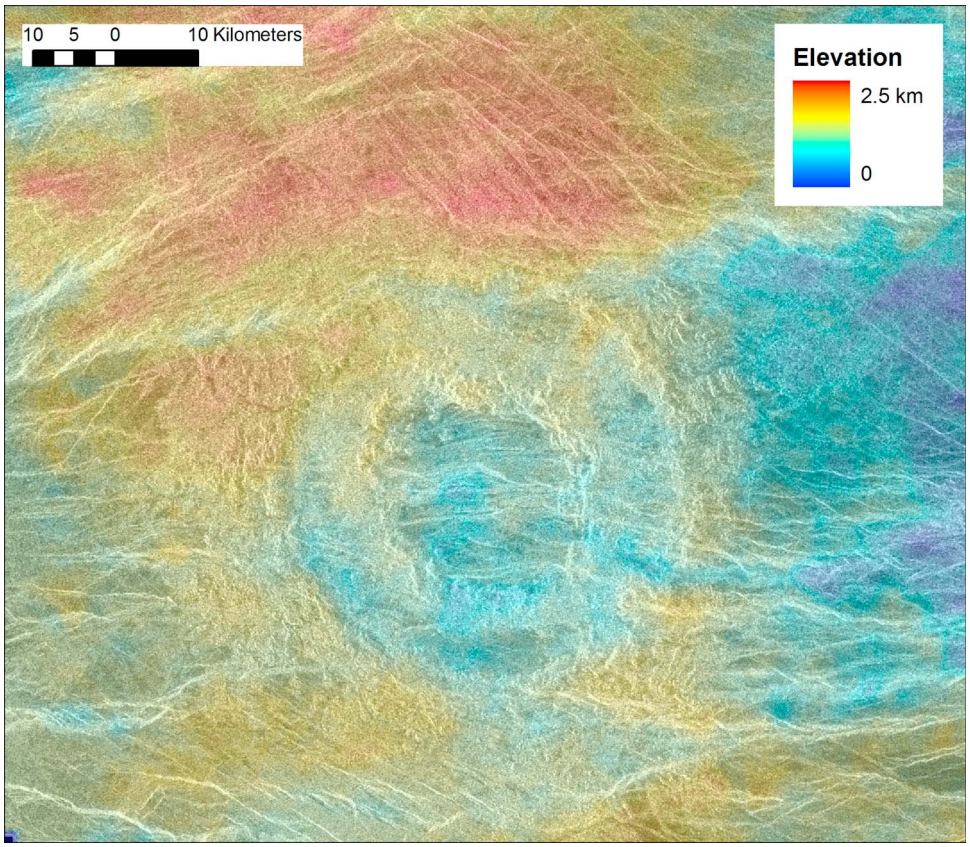

Figure 33. Imagery and stereo-derived topography for Langtry.

[82] Studies of the impact population, by themselves, cannot resolve the "directional, possibly catastrophic, evolution" versus "uniformitarian" debate regarding the resurfacing history of Venus. All of the craters combined only cover a small portion of the planet, so even if we had detailed geologic histories for every impact structure then we would still not have a complete picture for the planet's surface history. The area of the planet covered by the stereo imagery is limited and not necessarily representative of the remainder of the globe. Nevertheless, our work does place important constraints on the nature of suitable resurfacing hypotheses.

[83] We first discuss the general concept of using the Venusian crater population to date the surface. As discussed in the Introduction, crater counts can only be used to date surfaces that predate the craters. Our work indicates that calculations of a crater retention age for Venus should utilize only bright-floored craters, or about 20% of the population [*Herrick and Phillips*, 1994]. Using the *McKinnon et al.* [1997] estimate of cratering rate, this would place the mean surface age of Venus at ~150 My, a value comparable to the mean age of Earth's ocean basins.

[84] The entire population of craters can be considered as the age of some "basal" surface only if one makes the following assumptions:

[85] 1. There is some basal surface that was wiped crater free at some time in the past.

[86] 2. No craters have been completely covered or destroyed since that basal surface was created.

[87] If floor darkening and other crater modification were largely due to covering by minor surficial weathering and soil deposition, and/or postimpact volcanism was entirely confined to the crater floor, then these assumptions would be true and we could consider the entire population as giving a mean surface age for Venus, excluding minor later activity. This, in fact, has been the dominant post-Magellan view and is required by the surface dating methodology of *Basilevsky and Head* [2002b, 2002c]. Based on our work and mapping work by others [e.g., *Guest and Stofan*, 1999; *Stofan et al.*, 2005], we see little justification for either of these two assumptions. This does not mean that the dark-floored craters have no use in constraining the resurfacing history of Venus. Their near-random distribution certainly indicates some global uniformity in the rates of crater removal. Redoing three-dimensional modeling exercises of volcanic resurfacing [*Bullock et al.*, 1993; *Romeo and Turcotte*, 2010] with a much higher percentage of volcanically modified craters is also warranted.

[88] We now turn our attention to the different perspectives on the resurfacing history of Venus. If the directional evolution model is valid, then our work indicates that the evolution was slow and the timing of events overlapped considerably. The vast majority of Venusian impact craters have dark floors, and our work indicates that hundreds of meters of volcanic infilling is common. A valid end-member interpretation is that the crater population still represents a population emplaced on a mostly inactive planet, but the final throws of global emplacement of volcanic plains has filled most of the craters with a few hundred vertical meters of volcanic flows. If this is true, then posttessera plains emplacement must have dragged on for most of the visible

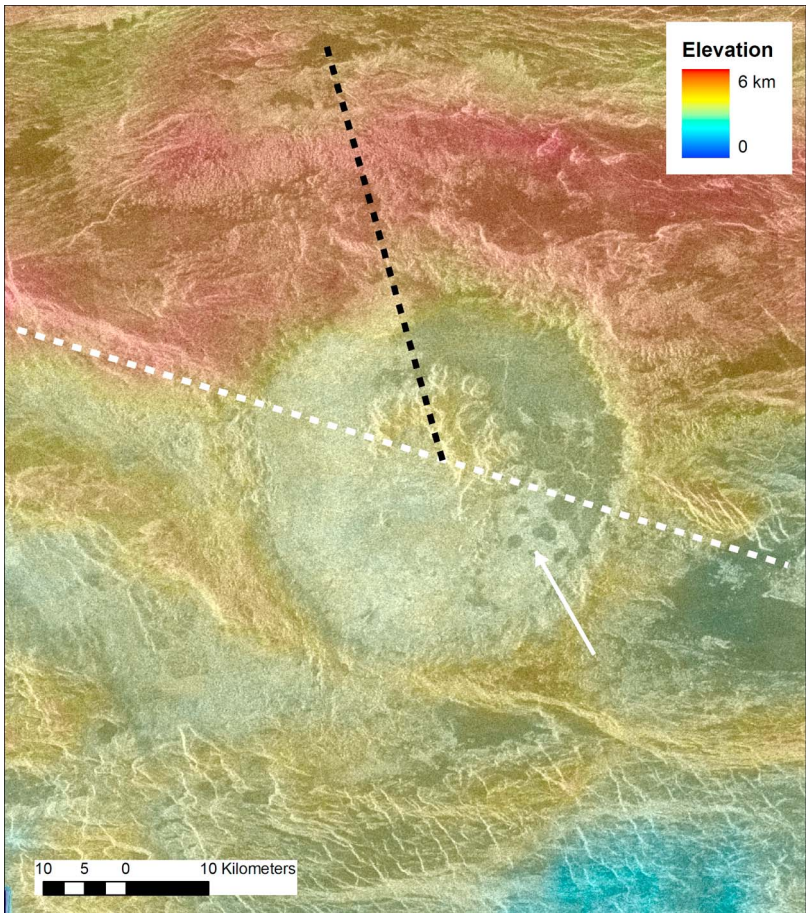

Figure 34. Imagery and stereo-derived topography for Warren (11.7°S, 176.5°E, D = 49 km). White dashed line shows strike of a fault that predates radar-bright flows that fill the crater. Crater rim and central structure are downdropped south of the fault. Arrow points to possible kipukas of radar-dark material. Black dashed line shows fault through rim and portion of central peak.

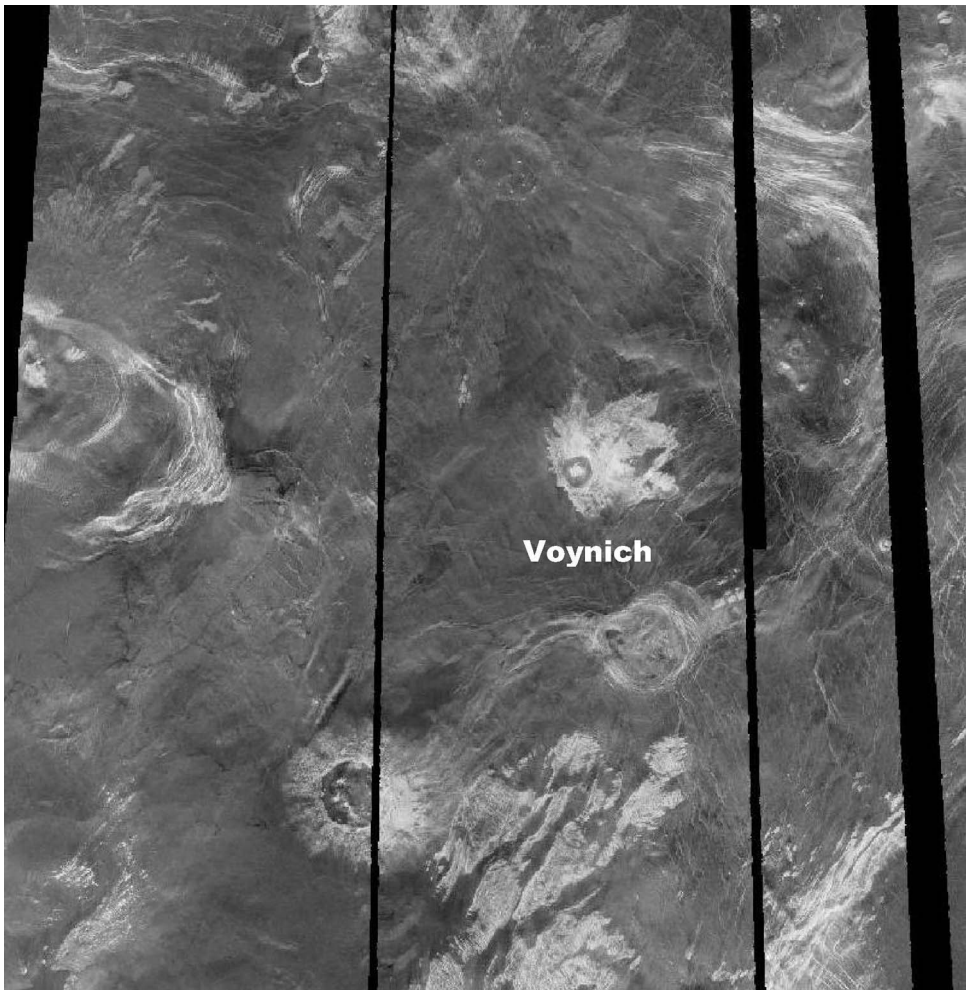

Figure 35. Regional view (1200 × 1200 km; 29 to 40.8°N, 47.9 to 62.1°E) showing Voynich in the regional plains surrounded by the volcanoes and corona of Bell Regio. Potanina is the larger crater to the southwest.

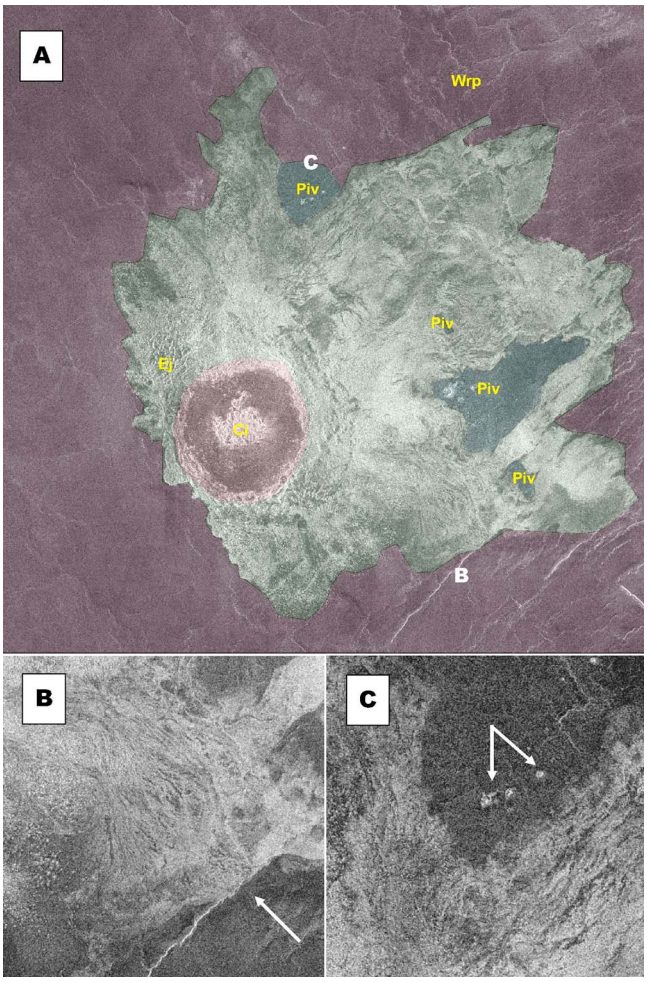

Figure 36. (a) Voynich crater (35.3°N, 56.1°E, D = 48 km); white letters indicate locations of insets. Map units are wrinkle ridged plains (Wrp), ejecta (Ej), crater interior (Ci), and postimpact volcanism (Piv). (b) Ejecta flows from Voynich are diverted by wrinkle ridge (arrow). (c) Small pits (arrows) are sources for radar-dark flows that superpose Voynich ejecta.

surface history of the planet. The detailed studies of the large craters indicates that the cessation of tessera deformation must have overlapped considerably with emplacement of the plains. Thus, while a tessera/plains/rifts evolution is a valid hypothesis within the context of the work presented here, that evolution could not have occurred as a "catastrophe" lasting less than several hundred million years.

[89] The highly varying levels of postimpact volcanism and deformation that the craters have experienced are consistent with a steady state model of Venus resurfacing. In this view, there is spatial variety in the removal processes, but all of the removal processes have operated throughout the visible surface history of the planet. Craters are in a variety of stages of being removed. Aside from the single exception of the rifted crater Balch in Beta Regio, no Venusian craters show enough horizontal strain to make a crater noncircular. While faulting may combine with volcanism to remove a crater, we see no progression that indicates that deformation alone is rendering craters unrecognizable on Venus. It still remains a powerful constraint that the distribution of geologic features on the planet (plains, volcanoes, rifts, etc.) is decidedly more nonuniform in distribution than the crater population. That means that while the nature of resurfacing on Venus may vary regionally in the uniformitarian hypothesis, the rates must be nearly similar.

[90] **Acknowledgments.** This work was supported by NASA grants to R.R.H. from the Planetary Geology and Geophysics Program. M.E.R.'s efforts were partially supported by an NSF-sponsored Research Experience for Undergraduates (REU) program administered by the Geophysical Institute at the University of Alaska Fairbanks. Tracy Gregg provided input to M.E.R.'s efforts while M.E.R. was an undergraduate at University at Buffalo (SUNY). We thank Ellen Stofan and two anonymous reviewers for insightful comments.

References

Arvidson, R. E., R. Greeley, M. C. Malin, R. S. Saunders, N. Izenberg, J. J. Plaut, E. R. Stofan, and M. K. Shepard (1992), Surface modification of Venus as inferred from Magellan observations of plains, *J. Geophys. Res.*, *97*, 13,303–13,317, doi:10.1029/92JE01384.

Basilevsky, A. T., and J. W. Head III (1995), Global stratigraphy of Venus: Analysis of a random sample of thirty-six test areas, *Earth Moon Planets*, *66*, 285–336, doi:10.1007/BF00579467.

Basilevsky, A. T., and J. W. Head III (1998), The geologic history of Venus: A stratigraphic view, *J. Geophys. Res.*, *103*, 8531–8544, doi:10.1029/98JE00487.

Basilevsky, A. T., and J. W. Head III (2000), Geologic units on Venus: Evidence for their global correlation, *Planet. Space Sci.*, *48*, 75–111, doi:10.1016/S0032-0633(99)00083-5.

Basilevsky, A. T., and J. W. Head III (2002a), On the rates and styles of late volcanism and rifting on Venus, *J. Geophys. Res.*, *107*(E6), 5041, doi:10.1029/2000JE001471.

Basilevsky, A. T., and J. W. Head III (2002b), Venus: Analysis of the degree of impact crater deposit degradation and assessment of its use for dating geological units and features, *J. Geophys. Res.*, *107*(E8), 5061, doi:10.1029/2001JE001584.

Basilevsky, A. T., and J. W. Head III (2002c), Venus: Timing and rates of geologic activity, *Geology*, *30*, 1015–1018, doi:10.1130/0091-7613(2002)030<1015:VTAROG>2.0.CO;2.

Basilevsky, A. T., and J. W. Head III (2006), Impact craters on regional plains on Venus: Age relations with wrinkle ridges and implications for the geological evolution of Venus, *J. Geophys. Res.*, *111*, E03006, doi:10.1029/2005JE002473.

Basilevsky, A. T., and B. A. Ivanov (1990), Cleopatra crater on Venus: Venera 15/16 data and impact/volcanic origin controversy, *Geophys. Res. Lett.*, *17*, 175–178, doi:10.1029/GL017i002p00175.

Basilevsky, A. T., and G. G. Schaber (1991), Cleopatra crater on Venus: Happy solution of the volcanic vs. impact crater controversy, *Lunar Planet. Sci.*, *XXII*, 59–60.

Basilevsky, A. T., J. W. Head, G. G. Schaber, and R. G. Strom (1997), The resurfacing history of Venus, in *Venus II: Geology, Geophysics, Atmosphere, and Solar Wind Environment*, edited by S. W. Bougher et al., pp. 667–694, Univ. of Ariz. Press, Tucson.

Basilevsky, A. T., J. W. Head, M. A. Ivanov, and V. P. Kryuchkov (1999), Impact craters on geologic units of northern Venus: Implications for the duration of the transition from tessera to regional plains, *Geophys. Res. Lett.*, *26*, 2593–2596, doi:10.1029/1999GL008329.

Brown, C. D., and R. E. Grimm (1996), Floor subsidence and rebound of large Venus craters, *J. Geophys. Res.*, *101*, 26,057–26,067, doi:10.1029/96JE02706.

Bullock, M. A., D. H. Grinspoon, and J. W. Head (1993), Venus resurfacing rates: Constraints provided by 3-D Monte Carlo simulations, *Geophys. Res. Lett.*, *20*, 2147–2152, doi:10.1029/93GL02505.

Campbell, B. A., and P. G. Campbell (2002), Geologic map of the Bell Regio Quadrangle (V-9), Venus, *U.S. Geol. Surv. Misc. Geol. Invest. Map, I-2743*.

Campbell, B. A., and P. G. Rogers (1994), Bell Regio, Venus: Integration of remote sensing data and terrestrial analogs for geologic analysis, *J. Geophys. Res.*, *99*, 21,153–21,171, doi:10.1029/94JE01862.

Campbell, D. B., N. J. S. Stacy, W. I. Newman, R. E. Arvidson, E. M. Jones, G. S. Musser, A. Y. Roper, and C. Schaller (1992), Magellan observations of extended impact crater related features on the surface of Venus, *J. Geophys. Res.*, *97*, 16,249–16,277, doi:10.1029/92JE01634.

Carter, L. M., D. B. Campbell, and B. A. Campbell (2004), Impact crater related surficial deposits on Venus: Multipolarization radar observations with Arecibo, *J. Geophys. Res.*, *109*, E06009, doi:10.1029/2003JE002227.

Cochrane, C. G., and R. C. Ghail (2006), Topographic constraints on impact crater morphology on Venus from high-resolution stereo synthetic aperture radar digital elevation models, *J. Geophys. Res.*, *111*, E04007, doi:10.1029/2005JE002570.

Collins, G. C., J. W. Head, A. T. Basilevsky, and M. A. Ivanov (1999), Evidence for rapid regional plains emplacement on Venus from the population of volcanically embayed impact craters, *J. Geophys. Res.*, *104*, 24,121–24,139, doi:10.1029/1999JE001041.

Guest, J. E., and E. R. Stofan (1999), A new view of the stratigraphic history of Venus, *Icarus*, *139*, 55–66, doi:10.1006/icar.1999.6091.

Hansen, V. L., and H. R. DeShon (2003), Geologic map of the Diana Chasma Quadrangle (V-37), Venus, *U.S. Geol. Surv. Misc. Geol. Invest. Map, I-2752*.

Hansen, V. L., and D. A. Young (2007), Venus's evolution: A synthesis, *Spec. Pap. Geol. Soc. Am.*, *419*, 255–273.

Herrick, R. R. (1994), Resurfacing history of Venus, *Geology*, *22*, 703–706, doi:10.1130/0091-7613(1994)022<0703:RHOV>2.3.CO;2.

Herrick, R. R., and N. K. Forsberg-Taylor (2003), The shape and appearance of craters formed by oblique impact on the Moon and Venus, *Meteorit. Planet. Sci.*, *38*, 1551–1578, doi:10.1111/j.1945-5100.2003.tb00001.x.

Herrick, R. R., and R. J. Phillips (1994), Implications of a global survey of Venusian impact craters, *Icarus*, *111*, 387–416, doi:10.1006/icar.1994.1152.

Herrick, R. R., and V. L. Sharpton (1996), Geologic history of the Mead impact basin, Venus, *Geology*, *24*, 11–14, doi:10.1130/0091-7613(1996)024<0011:GHOTMI>2.3.CO;2.

Herrick, R. R., and V. L. Sharpton (2000), Implications from stereo-derived topography of Venusian impact craters, *J. Geophys. Res.*, *105*, 20,245–20,262, doi:10.1029/1999JE001225.

Herrick, R. R., V. L. Sharpton, M. C. Malin, S. N. Lyons, and K. Feely (1997), Morphology and morphometry of impact craters, in *Venus II: Geology, Geophysics, Atmosphere, and Solar Wind Environment*, edited by S. W. Bougher et al., pp. 1015–1046, Univ. of Ariz. Press, Tucson.

Herrick, R. R., J. Dufek, and P. J. McGovern (2005), Evolution of large shield volcanoes on Venus, *J. Geophys. Res.*, *110*, E01002, doi:10.1029/2004JE002283.

Ivanov, M. A., and A. T. Basilevsky (1993), Density and morphology of impact craters on tessera terrain, Venus, *Geophys. Res. Lett.*, *20*, 2579–2582, doi:10.1029/93GL02692.

Ivanov, B. A., A. T. Basilevsky, V. P. Kryuchkov, and I. M. Chernaya (1986), Impact craters of Venus: Analysis of Venera 15 and 15 data, *J. Geophys. Res.*, *91*, D413–D430, doi:10.1029/JB091iB04p0D413.

Izenberg, N. R., R. E. Arvidson, and R. J. Phillips (1994), Impact crater degradation on Venusian plains, *Geophys. Res. Lett.*, *21*, 289–292, doi:10.1029/94GL00080.

Janes, D. M., S. W. Squyres, D. L. Bindschadler, G. Baer, G. Schubert, V. L. Sharpton, and E. R. Stofan (1992), Geophysical models for the formation and evolution of coronae on Venus, *J. Geophys. Res.*, *97*, 16,055–16,067, doi:10.1029/92JE01689.

Johnson, R. R. (1973), *Elementary Statistics*, 480 pp., Duxbury, Boston.

McKinnon, W. B., K. J. Zahnle, B. A. Ivanov, and H. J. Melosh (1997), Cratering on Venus: Models and observations, in *Venus II: Geology, Geophysics, Atmosphere, and Solar Wind Environment*, edited by S. W. Bougher et al., pp. 969–1014, Univ. of Ariz. Press, Tucson.

Namiki, N., and S. C. Solomon (1994), Impact crater densities on volcanoes and coronae on Venus: Implications for volcanic resurfacing, *Science*, *265*, 929–933, doi:10.1126/science.265.5174.929.

Phillips, R. J., G. G. Schaber, R. E. Arvidson, J. M. Boyce, D. B. Campbell, J. E. Guest, and L. A. Soderblom (1991), Initial analysis of Venus impact craters with Magellan data, *Science*, *252*, 288–297, doi:10.1126/science.252.5003.288.

Phillips, R. J., R. F. Raubertas, R. E. Arvidson, I. C. Sarkar, R. R. Herrick, N. Izenberg, and R. E. Grimm (1992), Impact crater distribution and the resurfacing history of Venus, *J. Geophys. Res.*, *97*, 15,923–15,948, doi:10.1029/92JE01696.

Price, M., and J. Suppe (1995), Constraints on the resurfacing history of Venus from the hypsometry and distribution of volcanism, tectonism, and impact craters, *Earth Moon Planets*, *71*, 99–145, doi:10.1007/BF00612873.

Reese, C. C., V. S. Solomatov, and C. P. Orth (2007), Mechanisms for cessation of magmatic resurfacing on Venus, *J. Geophys. Res.*, *112*, E04S04, doi:10.1029/2006JE002782.

Romeo, I., and D. L. Turcotte (2010), Resurfacing on Venus, *Planet. Space Sci.*, *58*, 1374–1380, doi:10.1016/j.pss.2010.05.022.

Schaber, G. G., R. C. Kozak, and H. Masursky (1986), Cleopatra crater on Venus: New evidence for a volcanic origin, *Lunar Planet. Sci.*, *XVII*, 762–763.

Schaber, G. G., H. J. Moore, R. G. Strom, L. A. Soderblom, L. R. Gaddis, J. M. Boyce, R. L. Kirk, D. J. Chadwick, and J. Russell (1992), The geology and distribution of impact craters on Venus: What are they telling us?, *J. Geophys. Res.*, *97*, 13,257–13,302, doi:10.1029/92JE01246.

Schultz, P. H. (1992), Atmospheric effects on ejecta emplacement and crater formation on Venus from Magellan, *J. Geophys. Res.*, *97*, 16,183–16,248, doi:10.1029/92JE01508.

Sharpton, V. L. (1994), Evidence from Magellan for unexpectedly deep complex craters on Venus, in *Large Meteorite Impacts and Planetary Evolution*, edited by B. O. Dressler et al., *Spec. Pap. Geol. Soc. Am.*, 293, 19–27.

Solomatov, V. S., and L.-N. Moresi (1996), Stagnant lid convection on Venus, *J. Geophys. Res.*, *101*, 4737–4753, doi:10.1029/95JE03361.

Stofan, E. R., A. W. Brain, and J. E. Guest (2005), Resurfacing styles and rates on Venus: Assessment of 18 venusian quadrangles, *Icarus*, *173*, 312–321, doi:10.1016/j.icarus.2004.08.004.

Strom, R. G., G. G. Schaber, and D. D. Dawson (1994), The global resurfacing of Venus, *J. Geophys. Res.*, *99*, 10,899–10,926, doi:10.1029/94JE00388.

Turcotte, D. L. (1993), An episodic hypothesis for Venusian tectonics, *J. Geophys. Res.*, *98*, 17,061–17,068, doi:10.1029/93JE01775.

Wichman, R. W. (1999), Internal crater modification on Venus: Recognizing crater-centered volcanism by changes in floor morphology and floor brightness, *J. Geophys. Res.*, *104*, 21,957–21,977.

R. R. Herrick, Geophysical Institute, University of Alaska Fairbanks, 903 Koyukuk Dr., Fairbanks, AK 99775-7320, USA. (rherrick@gi.alaska.edu)

M. E. Rumpf, Hawai'i Institute of Geophysics and Planetology, University of Hawai'i at Manoa, Honolulu, HI 96822, USA.